

LIMNOLOGY AND OCEANOGRAPHY

January 1997

Volume 42

Number 1

Limnol. Oceanogr., 42(1), 1997, 1–20
© 1997, by the American Society of Limnology and Oceanography, Inc.

Photosynthetic rates derived from satellite-based chlorophyll concentration

Michael J. Behrenfeld and Paul G. Falkowski

Oceanographic and Atmospheric Sciences Division, Brookhaven National Laboratory,
Upton, New York 11973-5000

Abstract

We assembled a dataset of ^{14}C -based productivity measurements to understand the critical variables required for accurate assessment of daily depth-integrated phytoplankton carbon fixation (PP_{eu}) from measurements of sea surface pigment concentrations (C_{sat}). From this dataset, we developed a light-dependent, depth-resolved model for carbon fixation (VGPM) that partitions environmental factors affecting primary production into those that influence the relative vertical distribution of primary production (P_z) and those that control the optimal assimilation efficiency of the productivity profile (P^B_{opt}). The VGPM accounted for 79% of the observed variability in P_z and 86% of the variability in PP_{eu} by using measured values of P^B_{opt} . Our results indicate that the accuracy of productivity algorithms in estimating PP_{eu} is dependent primarily upon the ability to accurately represent variability in P^B_{opt} . We developed a temperature-dependent P^B_{opt} model that was used in conjunction with monthly climatological images of C_{sat} , sea surface temperature, and cloud-corrected estimates of surface irradiance to calculate a global annual phytoplankton carbon fixation (PP_{annu}) rate of $43.5 \text{ Pg C yr}^{-1}$. The geographical distribution of PP_{annu} was distinctly different than results from previous models. Our results illustrate the importance of focusing P^B_{opt} model development on temporal and spatial, rather than the vertical, variability.

Thousands of measurements of marine phytoplankton productivity have been made at discrete locations throughout the world's oceans since the introduction of the radiolabelled carbon uptake method (i.e. ^{14}C method) in 1952 (Steemann Nielsen 1952). Although numerous, these discrete primary productivity measurements only provide information for infinitesimally small points over the oceans' surfaces. Scaling these discrete measurements to global projections by means of satellite-based estimates of chlorophyll concentration (C_{sat}) requires mathematical models that quantitatively relate primary productivity to chlorophyll (Bidigare et al. 1992).

Acknowledgments

We thank Monica Chen for global primary production calculations and images of productivity distributions, David Siegel for assistance with the BATS productivity data, Richard Barber for generously contributing the EQPAC data, William Behrens for assistance with the BNL database, and Jay O'Reilly for the MARMAP contribution to the dataset. We especially thank André Morel for the LPCM data, the source code for his bio-optical model, and numerous helpful discussions. We also thank Peter Minnett and Kevin Turpie for assistance with data retrieval and analysis and Creighton Wirick, Zbigniew Kolber, and two anonymous reviewers for helpful recommendations and discussions.

This research was supported by the U.S. National Aeronautics and Space Administration grant UPN161-35-05-08 and by the U.S. Department of Energy contract DE-AC02-76CH00016.

This manuscript is dedicated to William Winner for his inspiration and friendship.

The simplest productivity models estimate time- and depth-integrated primary production as a function of sea surface chlorophyll (e.g. Smith et al. 1982; Eppley et al. 1985). The next step in algorithm complexity introduces surface irradiance as a second factor controlling productivity, where depth-integrated production is the product of depth-integrated chlorophyll, daily surface irradiance, and a constant, water-column averaged quantum yield (Ψ) for photosynthesis (Morel 1978; Falkowski 1981; Platt 1986; Morel 1991). Diverse empirical relationships also exist that relate depth-integrated production to C_{sat} , euphotic depth, and a photoadaptive parameter (see Balch et al. 1992). A more mechanistic approach to productivity modeling has been attempted by use of complex bio-optical models (Platt and Sathyendranath 1988; Morel and Berthon 1989; Morel 1991; Platt et al. 1991). Bio-optical models attempt to improve productivity estimates over the depth-integrated empirical relationships by including model variables that account for the spectrally dependent attenuation of photosynthetically active radiation (PAR, 400–700 nm) through the water column, as well as vertical and spatial variability in phytoplankton optical absorption cross sections (a^*) and photosynthesis vs. irradiance (P vs. E) parameters (α , P^B_{max} , β).

An advantage of bio-optical models is that they account for the variable fraction of the euphotic zone that is light-saturated. However, it is not clear how much of the added complexity in bio-optical models reflects the level of under-

standing about a particular variable rather than the importance of the exact representation of the variable on the predictive capacity of the model. At all levels of complexity, productivity models often perform well in predicting integrated productivity when comparisons are limited to the datasets from which they were derived. However, when these models are used to predict column productivity from different datasets, model performance is often dramatically reduced (Campbell and O'Reilly 1988; Balch et al. 1992). Clearly, some of the disagreement between modeled and measured production is due to methodological differences in ^{14}C measurements and errors in the ^{14}C data, but much of the discrepancy must also result from limitations of the models.

To better understand the level of complexity and the critical factors required for making reliable estimates of daily integrated phytoplankton production based on C_{sat} , we investigated the variability observed in phytoplankton primary production by assembling a dataset of 11,283 ^{14}C -based measurements of daily carbon fixation collected at 1,698 oceanographic stations in both open ocean and coastal waters. The dataset includes measurements that have previously been used for testing productivity models, as well as previously unutilized data.

By removing the influences of euphotic depth, photoperiod, and chlorophyll concentration, we discovered a consistent trend in the vertical distribution of primary production. We therefore developed an irradiance-dependent, depth-resolved productivity model that accounted for the observed vertical trends in normalized productivity. Parameters of the model were established with data from a single research program and model performance was tested with the full ^{14}C dataset. We then simplified the model by removing the vertical resolution, thereby allowing rapid assessment of depth-integrated estimates of euphotic zone productivity. We identified a key parameter, P_{opt}^B , required for modeling phytoplankton primary production and developed a preliminary model for estimating P_{opt}^B . By knowing P_{opt}^B alone, our vertically generalized production model (VGPM) accounts for 86% of the observed variability in measured values of daily integral production. When P_{opt}^B is estimated by means of the relationship developed from the dataset, the VGPM accounts for 58% of the observed variability. We applied the VGPM to monthly coastal zone color scanner C_{sat} images to estimate annual global primary production and to compare results using our P_{opt}^B model, in terms of the distribution and total primary production, to similar calculations from other primary production models. These results have implications for future development of satellite-based models of global oceanic primary production.

Methods

Table 1 summarizes the source, location, and number of stations for all productivity measurements used for model development and testing. We extracted 272 productivity profiles from the oceanographic database at Brookhaven National Laboratory, 141 profiles from the JGOFS database, 243 profiles from the algorithm testing database of André

Morel at Laboratoire de Physique et Chimie Marines (LPCM, Université Paris 6) and 1,042 profiles from the NOAA MARMAP database (O'Reilly and Busch 1984; O'Reilly et al. 1987). The complete dataset includes productivity measurements from both case 1 and case 2 waters (Morel and Prieur 1977), from oligotrophic gyre regions to highly productive upwelling regions, from 80°N to 70°S , and from all major ocean basins. ^{14}C measurements included both in situ and simulated in situ incubations, with incubation durations ranging from 2 to 24 h (<3% of the ^{14}C data was derived from incubations <6 h). In addition to ^{14}C uptake data, the dataset includes vertical profiles of chlorophyll concentration (mg Chl m^{-3})—mostly measured with fluorometric techniques (Holm-Hansen et al. 1965) or HPLC methods—daily integrated molar photon flux of surface PAR, euphotic depth (Z_{eu}), incubation irradiance as percentage of surface irradiance, latitude, longitude, date, and, when available, sea surface temperature ($^\circ\text{C}$).

The dataset includes productivity measurements collected between 1971 and 1994. The preferred ^{14}C method for measuring primary production has varied during this period and between investigators. Thus, to avoid investigator-dependent variability between productivity values, we developed the productivity model from the largest available methodologically consistent database, that of the MARMAP program. Restricting model development to MARMAP data alone also allowed us to test algorithm performance with an independent dataset. Because the MARMAP data contribute to more than half of the productivity profiles included in the full dataset, we report separate statistics for the full dataset, MARMAP data alone, and all other data for comparisons between measured and modeled daily integrated productivity values, except when sea surface temperature is required for calculations, as these data are limited. Radiometric measurements or Secchi depth estimates of Z_{eu} were used in all calculations of depth-integrated primary production.

Results

Depth-integrated primary production (PP_{eu}) and chlorophyll concentration for the full dataset ranged from 30 to 8,543 $\text{mg C m}^{-2} \text{d}^{-1}$ and from 3 to 437 mg Chl m^{-2} (a list of notations is provided). For the full dataset, 38% of the observed variability in PP_{eu} was accounted for by the product of surface chlorophyll (C_{z_0}) and euphotic depth (Z_{eu}). The correlation between PP_{eu} and the product of C_{z_0} and Z_{eu} was reduced to 29% by means of logarithmic transformation of the data, indicating an even poorer relationship at low chlorophyll concentrations. Including surface irradiance (E_0) in the calculation (i.e. $C_{z_0} \times Z_{\text{eu}} \times E_0$) only marginally improved the correlation between measured and modeled production to 42%. Thus, for our dataset, less than half of the observed variability in primary production would be accounted for by depth-integrated chlorophyll alone or a Ψ -type model with constant proportionality (e.g. Falkowski 1981).

Vertical distributions of daily primary production (P_z , $\text{mg C m}^{-3} \text{d}^{-1}$) were investigated to identify sources of variability in PP_{eu} . Although P_z varied greatly between stations

Table 1. Sources for all ^{14}C measurements included in the dataset for model development and testing.

Source*	Program/ship	Month	Year	Location	No. of Sta.
BNL	<i>Atlantis</i>	Mar–Apr	1975, 78	NW Atlantic	20
	<i>Eastward</i>	Apr	1976	NW Atlantic	15
	<i>Keltz</i>	Mar	1976, 77	NW Atlantic	8
	<i>Henlopen</i>	Nov	1977	NW Atlantic	2
	<i>Knorr</i>	Aug	1977, 80	NW Atlantic	49
	<i>Argus</i>	Mar	1978	NW Atlantic	17
	<i>Delaware II</i>	Jun	1978	NW Atlantic	5
	<i>Albatros</i>	Mar	1979	NW Atlantic	8
	MESEX I	May	1979	NW Atlantic	5
	SEEP II	Feb–Nov	1988, 89	NW Atlantic	32
	NEWP	Jul	1992	Greenland shelf	37
	GYRE	May	1993	Sargasso Sea	5
	<i>Iselin</i>	Mar	1994	NW Atlantic	8
	Other				61
	JGOFS	BATS	Jan–Dec	1988–91	Sargasso Sea
HOTS		Jan–Dec	1989–93	Central North Pacific	38
EQPAC		Feb–Oct	1992	Equatorial Pacific	56
EUMELI		Jun	1992	Mauritanian upwelling/Sargasso Sea	13
LPCM	Mediproduct 1	Apr	1969	NW Mediterranean	13
	<i>Discoverer</i>	May	1970	Sargasso Sea, Gulf of Mexico, tropical eastern Pacific	24
	Cineca 2	Mar	1971	Mauritanian upwelling	16
	Mediproduct 3	Jun	1972	NW Mediterranean	13
	Cineca 5	Mar–Apr	1974	Mauritanian upwelling	12
	Joint 1	Mar	1974	Mauritanian upwelling	22
	Guidome	Sep	1976	Guinea Dome Zone	6
	Joint 2	Mar	1976	Peruvian upwelling	85
	Antiproduct 1	Mar	1977	South Indian/Antarctic zone	26
	Paciproduct	Sep	1986	Peruvian upwelling/Galapagos	11
	Chlomax	Sep	1987	Sargasso Sea	7
Mediproduct 6	Jun	1990	SW Mediterranean	8	
NOAA	MARMAP	Jan–Dec	1977–82	NW Atlantic	1,042

* Sources of productivity: BNL—Brookhaven National Laboratory; JGOFS—Joint Global Ocean Flux Study; LPCM—Laboratoire de Physique et Chimie Marines (André Morel); NOAA—National Oceanic and Atmospheric Administration.

(Fig. 1A), much of this variability could be attributed to three basic factors: chlorophyll concentration at each depth (C_z), photoperiod (D_{irr}), and optical depth (ζ) corresponding to the incubation irradiance [note that ζ is the absolute value for the product of physical depth (z) and the mean attenuation coefficients for PAR (K_{avg})]. Accounting for these three factors resulted in consistent patterns in the normalized P_z (Fig. 1B) that emphasize the importance of irradiance—exhibiting regions of light limitation, light saturation, and, at high light intensities, photoinhibition. Based on these observed patterns (Fig. 1B), we developed a model for estimating PP_{cu} by constructing an irradiance-dependent function describing the relative vertical distribution of production (P^B_ζ). We then converted P^B_ζ into P_z by using a second scaling function for estimating the maximum P_z (P^B_{opt}) for each profile.

Relative vertical distribution model—Observed patterns in P^B_ζ (dimensionless) were modeled as a function of daily solar irradiance as

$$P^B_\zeta = [1 - \exp(-E_\zeta/E_{max})]\exp(-\beta_d \times E_\zeta), \quad (1)$$

where E_ζ is irradiance at a given ζ ; E_{max} is irradiance at the inflection point between light limitation and light saturation in the absence of photoinhibition and is calculated from E_{opt} , the irradiance corresponding to P^B_{opt} (see below); and β_d is the variable slope for photoinhibition at daily irradiances $>E_{opt}$. PP_{cu} is thus calculated from Eq. 1 by scaling P^B_ζ to P^B_{opt} and C_z , converting ζ to absolute depths, and multiplying by D_{irr} .

The P^B_ζ model (Eq. 1), when scaled to P^B_{opt} , is nearly identical in form to the P vs. E equation (Platt et al. 1980; McBride 1992):

$$P = P_{max}[1 - \exp(-E/E_k)]\exp(-\beta E/P_{max}). \quad (2)$$

However, variable names differ between Eq. 1 and 2 because P vs. E variables (P_{max} , β , E_k) are measured under conditions of constant irradiance and have strict physiological interpretations, whereas P^B_ζ variables and P^B_{opt} are measured under irradiance conditions that can vary from light-limiting to

Notation

Environmental variables	
C_{z0}	Measured Chl concn at depth nearest the surface, mg Chl m^{-3}
C_{sat}	Surface Chl concn derived by satellite, mg Chl m^{-3}
C_z	Chl concn at depth z , mg Chl m^{-3}
D_{irr}	Photoperiod, decimal hours
E_0	Sea surface daily PAR, mol quanta m^{-2}
K_{avg}	Mean optical attenuation coefficient for PAR, m^{-1}
ζ	Optical depth; calculated as the product of K_d and depth z
Z_{cu}	Physical depth receiving 1% of E_0 , m
Physiological variables	
τ	Minimal electron turnover time of photosynthesis
n	Number of functional photosynthetic units
α	Initial slope of a P vs. E curve describing light-limited photosynthesis
β	P vs. E variable describing rate of PS2 damage as a function of irradiance
P_{max}^B	Chl-normalized maximum rate of C fixation, mg C (mg Chl) $^{-1}$ h^{-1}
E_k	Unique point on P vs. E curve where $\alpha \times$ irradiance = P_{max}^B , μ mol quanta m^{-2} h^{-1}
Model variables	
P_{opt}^B	Maximum C fixation rate within a water column, mg C (mg Chl) $^{-1}$ h^{-1}
ζ_{opt}	Optical depth of P_{opt}^B
C_{opt}	Chl concn at P_{opt}^B
E_{opt}	Daily PAR at ζ_{opt} , mol quanta m^{-2}
E_{max}	Daily PAR at the inflection point between light limitation and light saturation in the absence of photoinhibition, mol quanta m^{-2}
E_{ζ}	Daily PAR at ζ , mol quanta m^{-2}
P_{ζ}^B	Relative vertical distribution of C fixation as a function of ζ , dimensionless
P_z	C fixation at depth z , mg C (mg Chl) $^{-1}$ h^{-1}
P_{inh}	Percentage decrease between P_0^B and P_{opt}^B
β_d	Photoinhibition slope resulting in the observed relationship between E_0 and P_{inh}
PP_{cu}	Daily C fixation integrated from the surface to Z_{cu} , mg C m^{-2}
PP_{annu}	Annual phytoplankton C fixation in the oceans, Pg yr^{-1}
PP_{season}	Phytoplankton C fixation in the oceans (Pg C) during winter (December–February), spring (March–May), summer (June–August), and autumn (September–November)

photoinhibiting over the course of an incubation. E_k (Eq. 2) is equal to P_{max}^B/α and is independent of measurement irradiances (E). In contrast, E_{max} is a linear function of E_0 , owing to the effects of photoinhibition on E_{opt} . β_d differs from, and is always less than, the photoinhibition slope (β) of the P vs. E curve (McBride 1992; Henley 1993) when determined for the same phytoplankton assemblage because field measurements of β_d include periods of light limitation during the incubation. Finally, P_{max}^B is defined as the maximum rate of photosynthesis at saturating irradiance, which is controlled by the capacity of the Calvin cycle reactions and is proportional to the number of functional photosynthetic reaction centers (n) and their turnover rates (Falkowski 1980; Suke-

nik et al. 1987; Orellana and Perry 1992). In contrast, P_{opt}^B is the biomass-specific daily photosynthetic rate at the optimal ζ where the loss of potential carbon fixation due to photoinhibition is balanced by the loss due to increased time at subsaturating light intensities at greater depths. This balance between light limitation and photoinhibition at P_{opt}^B causes E_{opt} to increase with increasing E_0 . In the absence of photoinhibition, P_{opt}^B would always occur at the surface, where the maximum fraction of the photoperiod is spent at P_{max}^B . Differences between P_{max}^B and P_{opt}^B were also recognized by Rodhe et al. (1958) and Wright (1959) (they used the variables R_{opt} and a_{opt} , respectively).

P_{ζ}^B model parameters—The three light-dependent P_{ζ}^B variables— E_{opt} , E_{max} , and β_d (Eq. 1)—were parameterized with MARMAP productivity profiles normalized to C_z , ζ , and D_{irr} . The relationship between observed median surface photoinhibition (P_{inh}) and E_0 was (Fig. 2A)

$$P_{inh} = -0.0204E_0^2 + 2.515E_0 - 6.675 \quad \text{when } E_0 > 3 \text{ mol quanta } m^{-2} \text{ d}^{-1}. \quad (3)$$

P_{inh} is the percentage decrease in chlorophyll-normalized carbon fixation at the surface relative to P_{opt}^B ($P_{inh} = 0$ when $E_0 \leq 3$ mol quanta m^{-2} d^{-1}). Likewise, the median optical depth of P_{opt}^B (ζ_{opt}) increased with increasing E_0 owing to photoinhibition (Fig. 2B):

$$\zeta_{opt} = -7.56 \times 10^{-8}E_0^4 + 1.84 \times 10^{-5}E_0^3 - 0.00171E_0^2 + 0.075E_0 - 0.00137. \quad (4)$$

E_{opt} is calculated from Eq. 4 following the relationship between E_0 and light attenuation with depth (Fig. 2C):

$$E_{opt} = E_0 \times \exp(-\zeta_{opt}). \quad (5)$$

Equation 5 results in a positive slope for E_{opt} because photosynthetic quantum yields decrease with increasing E_0 owing to light saturation and photoinhibition. Finally, Eq. 3–5 were used in conjunction with Eq. 1 to solve for the irradiance-dependence of E_{max} and β_d , resulting in the observed relationship between E_0 and P_{inh} , ζ_{opt} , and E_{opt} (Fig. 2C):

$$\beta_d = -0.0203 \times \ln(E_0) + 0.124 \quad \text{when } E_0 > 3 \text{ mol quanta } m^{-2} \text{ d}^{-1}$$

$$\beta_d = 0.1 \quad \text{when } E_0 \leq 3 \text{ mol quanta } m^{-2} \text{ d}^{-1} \quad (6)$$

and

$$E_{max} = 0.3195E_0, \quad (7)$$

where $E_{max} > E_{opt}$ at $E_0 > 30$ mol quanta m^{-2} d^{-1} due to the normalization of P_{ζ}^B to 1 at P_{opt}^B . Variability in PP_{cu} resulting from irradiance-dependent changes in the vertical distribution of production is thus accounted for by means of the P_{ζ}^B model (Eq. 1) given parameters in terms of E_0 by Eq. 4–7. The resultant P_{ζ}^B profiles (Fig. 3A) closely approximate measured P_z profiles normalized to C_z , ζ , D_{irr} , and P_{opt}^B (Fig. 3B).

Conversion of P_{ζ}^B to P_z for calculating PP_{cu} requires an estimate of C_z , which we modeled from measurements of C_{z0} using the Gaussian distributions described by Morel and Berthon (1989). The vertically resolved model for calculating PP_{cu} (mg C m^{-2} d^{-1}) is thus

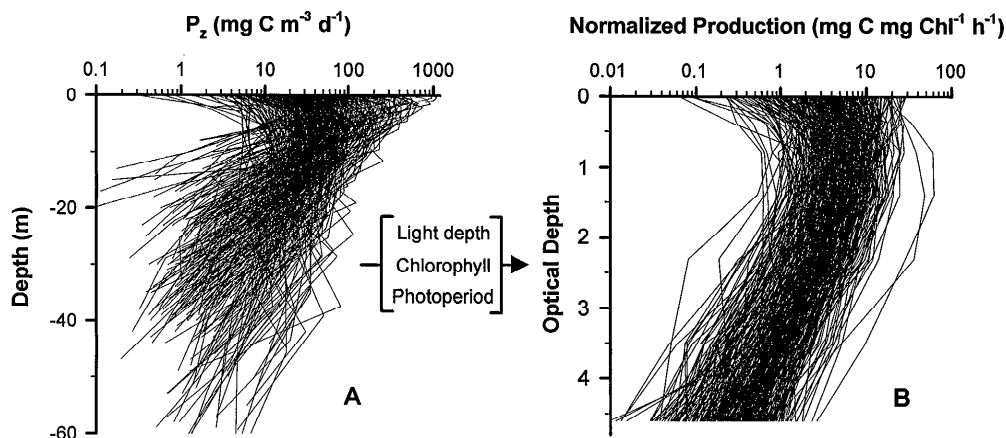


Fig. 1. Profiles of phytoplankton carbon fixation for 500 randomly chosen stations from the MARMAP dataset. A. A large degree of variability was observed in the vertical distributions of daily primary production (P_z , $\text{mg C m}^{-3} \text{d}^{-1}$). B. Normalizing P_z in panel A to chlorophyll concentration at each depth, photoperiod, and optical depth resulted in a consistent pattern in the vertical structure of productivity, which was modeled as a function of surface irradiance by the structural components of the VGPM (Eq. 8).

$$\begin{aligned}
 PP_{\text{eu}} &= P_{\text{opt}}^B \times D_{\text{irr}} \\
 &\times \int_{z=0}^{Z_{\text{eu}}} \frac{[1 - \exp(-E_z/E_{\text{max}})] \exp(\beta_d \times E_z)}{[1 - \exp(-E_{\text{opt}}/E_{\text{max}})] \exp(\beta_d \times E_{\text{opt}})} \\
 &\times C_z \times dz, \quad (8)
 \end{aligned}$$

where $E_z = E_0 \times \exp[-\ln(0.01)/Z_{\text{eu}} \times z]$. The two principal components of Eq. 8 are the structural elements composing the integral and the scaling factor, P_{opt}^B . To test the structural portion of the model, we compared observed values of P_z to modeled values calculated from Eq. 8 by using measured values of P_{opt}^B and E_0 . For this comparison, D_{irr} was calculated by using the date and location of each station and C_z was estimated from C_{z0} (Morel and Berthon 1989). In this manner, the model (Eq. 8) accounted for 79% ($n = 10,857$) of the observed vertical and spatial variability in P_z ($r^2 = 0.78$ for \log_{10} -transformed data) (Fig. 4).

The VGPM described by Eq. 8 permits calculation of E_0 -dependent changes in P_z by means of a simple formulation that requires estimation of far fewer input variables than do the bio-optical models. However, it would be computationally beneficial to remove the vertical resolution of the VGPM for applications that simply require estimates of PP_{eu} and not P_z (e.g. global-scale calculations using remote sensing data). The P_{opt}^B model can be simplified into a single equation describing the irradiance-dependent changes in depth-integrated, biomass-specific production if the scaling of P_{opt}^B by the Gaussian distributions of C_z can be replaced by a simple scaling to the chlorophyll concentration at P_{opt}^B (i.e. C_{opt}). Comparisons between modeled and measured PP_{eu} with and without C_z distributions indicated that including the vertical structure of chlorophyll did not statistically improve the predictive capacity of the model ($P \gg 0.1$). Thus, C_z can be removed from Eq. 8 and replaced by C_{opt} outside of the integral without loss of model performance when estimating PP_{eu} . Without the C_z requirement, the P_{opt}^B model can be reduced to

$$\int_z P_{\text{opt}}^B = [E_0/(E_0 + 4.1)], \quad (9)$$

which describes the relative change in the quantum efficiency of depth-integrated primary productivity ($\int_z P_{\text{opt}}^B$) as a function of E_0 . The significance of Eq. 9 is that it describes the relative change in the light-saturated fraction of the euphotic zone as a function of E_0 and illustrates one reason why the water-column-averaged quantum yield, Ψ , is not constant.

Simplifying the VGPM (Eq. 8) by using Eq. 9, replacing C_z by C_{opt} , and combining scaling factors for C_z and $\int_z P_{\text{opt}}^B$ results in the reduced VGPM for PP_{eu} ($\text{mg C m}^{-2} \text{d}^{-1}$):

$$\begin{aligned}
 PP_{\text{eu}} &= 0.66125 \times P_{\text{opt}}^B \times [E_0/(E_0 + 4.1)] \\
 &\times Z_{\text{eu}} \times C_{\text{opt}} \times D_{\text{irr}}. \quad (10)
 \end{aligned}$$

By removing the vertical resolution, the VGPM now resembles a suite of empirical relationships previously described for estimating PP_{eu} (e.g. Ryther and Yentsch 1957; Talling 1957; Bannister 1974; Smith and Baker 1978; Lewis et al. 1987; Balse and Yong 1990; Balch and Byrne 1994), with the addition of the irradiance-dependent term described by Eq. 9. The most recent of these studies (i.e. Balch and Byrne 1994) relates PP_{eu} to the function $P_{\text{max}}/K_{\text{avg}}$, where P_{max} can be equated to the product of P_{opt}^B , C_{opt} , and D_{irr} in Eq. 10 and K_{avg} is related to Z_{eu} [i.e. $K_{\text{avg}} = \ln(0.01)/Z_{\text{eu}}$]. For our dataset, the $P_{\text{max}}/K_{\text{avg}}$ function of Balch and Byrne (1994) explained 72% of the observed variability in PP_{eu} ($n = 1,698$) when calculations were made with measured values of P_{max} and K_{avg} [this correlation is nearly identical to the r^2 of 0.73 reported by Balch and Byrne (1994) for their independent dataset of 2,118 measurements] (Fig. 5A). The simplified VGPM (Eq. 10) improves the correlation between modeled and measured PP_{eu} to 86% for the entire dataset ($n = 1,698$) by using measured values of P_{opt}^B and Z_{eu} [89% for the MARMAP data ($n = 1,042$), 85% for all other data ($n = 656$)] (Fig. 5B). Logarithmic transformation increases this correlation to 87% (89% for the MARMAP data, 86%

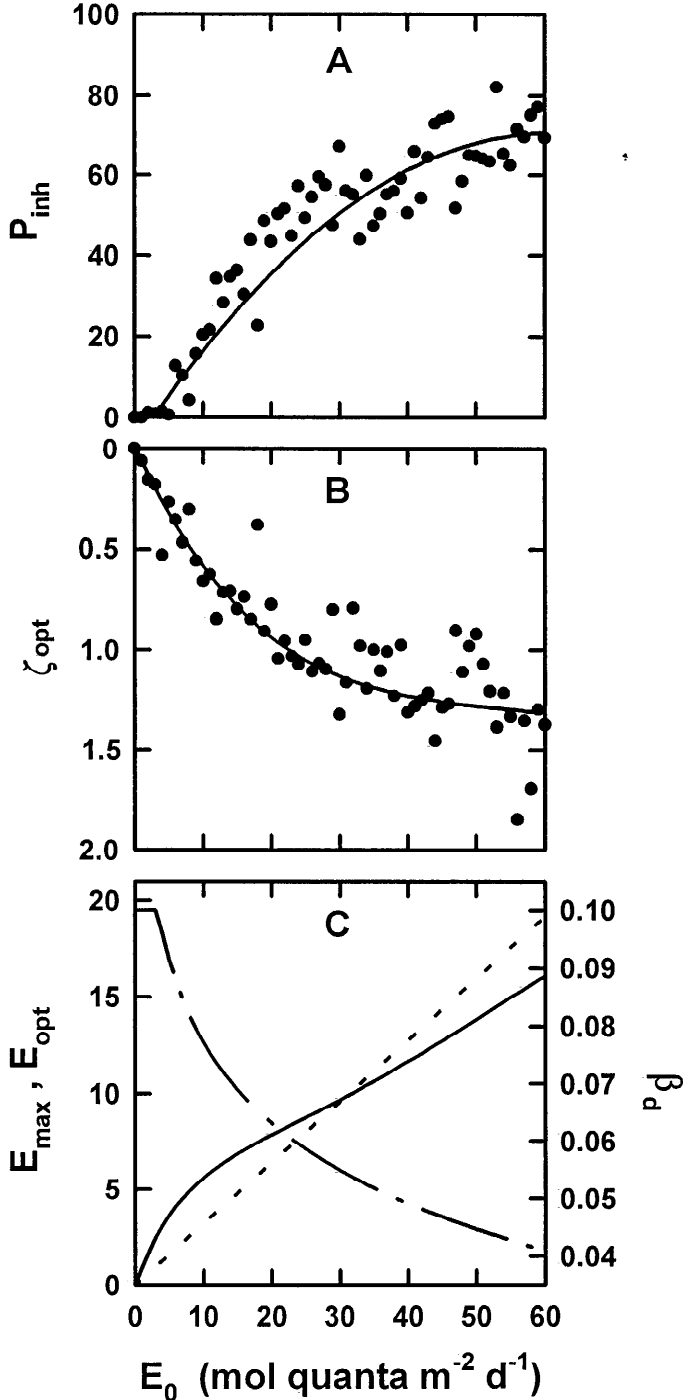


Fig. 2. A,B. Observed relationships between daily surface PAR (E_0) and median surface photoinhibition (P_{inh}) and median optical depth of P^B_{opt} (ζ_{opt}). P_{inh} was calculated as the percentage decrease in carbon fixation between the surface sample and P^B_{opt} . Polynomial fits (—) to the observational data in panels A and B are described by Eq. 3 and 4, respectively. C. Three light-dependent variables (E_{max} , E_{opt} , β_d) used in Eq. 1 to describe the relative vertical distribution of primary production (P^B_{c}). —, daily PAR at P^B_{opt} (i.e. E_{opt}) as calculated from ζ_{opt} with Eq. 5. - - -, irradiance-dependent photoinhibition (β_d) derived from panel A and described by Eq. 6. - · - ·, inflection point between light-limitation and light-saturation in the absence of photoinhibition (E_{max}) as described by Eq. 7.

for all other data) and indicates that model performance is maintained throughout the range of chlorophyll concentrations (Fig. 5C).

Computational advantages of reducing the vertically resolved VGPM (Eq. 8) to the simplified model (Eq. 10) would be limited if C_z profiles were still necessary for estimating C_{opt} from C_{z0} . However, C_{opt} is highly correlated with C_{z0} ($r^2 = 0.96$; 0.94 for \log_{10} -transformed data) (Fig. 6) owing to the near-surface location of P^B_{opt} ($\zeta_{\text{opt}} < 1.3$) for the entire range of E_0 (Fig. 2B). Thus, C_{opt} in Eq. 10 can be replaced by C_{z0} or remotely sensed surface chlorophyll (C_{sat}) for purposes of scaling P^B_{opt} .

Modeling P^B_{opt} —Modeling PP_{eu} with the VGPM requires measurement data or estimates for five input variables, namely P^B_{opt} , E_0 , Z_{eu} , C_{opt} , and D_{irr} . For remote-sensing applications, the latter four variables can be directly related to C_{sat} or calculated using radiative transfer models and measurements of cloud cover (errors in these calculations are discussed below). However, no method is currently available for directly measuring the photoadaptive parameter, P^B_{opt} , and thus relationships are required to relate P^B_{opt} to other environmental parameters that can be detected remotely, such as sea surface temperature (SST).

Relating P^B_{opt} to SST is justified from the physiological perspective that P^B_{opt} varies primarily as a function of P^B_{max} (Sukenik et al. 1987; Orellana and Perry 1992), which is regulated by Calvin cycle enzymatic activity (Falkowski 1980; Sukenik et al. 1987) and hence is temperature-dependent. P^B_{opt} is also influenced by light-limited (α) and photoinhibited (β) carbon fixation rates, but these effects are of secondary importance to P^B_{max} . The near-surface location of P^B_{opt} ensures that SST measurements provide acceptable estimates of the temperature at ζ_{opt} . Thus, the median value of P^B_{opt} was calculated for each 1°C temperature increment from -1 to 29°C for the 1,041 stations in our dataset that included SST information. Median P^B_{opt} was lowest at temperatures $< 1^\circ\text{C}$ and increased rapidly between 1 and 20°C , with a slight shoulder between 4 and 9°C (Fig. 7). Above 20°C , however, a sharp decrease in P^B_{opt} was observed (Fig. 7). This decrease in P^B_{opt} above 20°C was unexpected, based on the adaptive capacity of algae to increasing growth temperatures (Li 1980), and may be related to the association of high SST with regions of strong vertical stratification and nutrient-limiting conditions for phytoplankton growth (Zentara and Kamykowski 1977; Kamykowski and Zentara 1986; Balch and Byrne 1994).

A preliminary empirical model for estimating P^B_{opt} was parameterized from the observed relationship between median P^B_{opt} and temperature (T) as (Fig. 7)

$$P^B_{\text{opt}} = -3.27 \times 10^{-8} T^7 + 3.4132 \times 10^{-6} T^6 - 1.348 \times 10^{-4} T^5 + 2.462 \times 10^{-3} T^4 - 0.0205 T^3 + 0.0617 T^2 + 0.2749 T + 1.2956. \quad (11)$$

This high-order polynomial is well behaved for SST ranging from -1 to 29°C , but should not be generalized to temperatures outside this range. Equation 11 thus provides a single-factor model for estimating P^B_{opt} that can be used in conjunction with the VGPM for estimating PP_{eu} from SST, C_{sat} , and E_0 . For the reduced dataset where SST was available (n

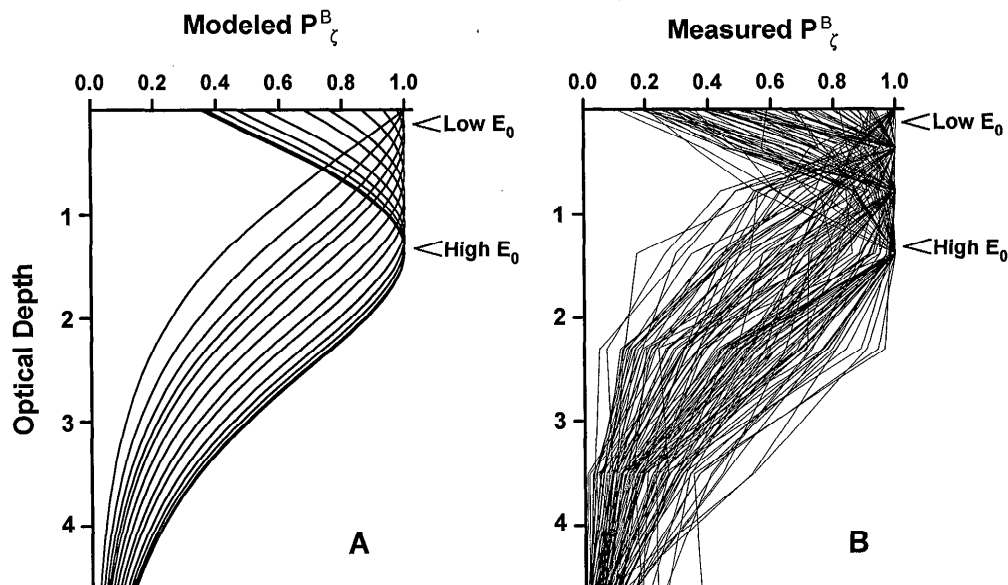


Fig. 3. Modeled and measured relative vertical distributions of primary production (P_z^B) (dimensionless) as a function of optical depth for a surface PAR (E_0) ranging from 2 to 60 mol quanta $m^{-2} d^{-1}$. P_z^B was modeled in panel A with Eq. 1 and parameters of E_0 from Eq. 4–7. P_z^B was calculated in panel B from measured productivity profiles by dividing by chlorophyll concentration at each depth, photoperiod, and the photoadaptive parameter, P_{opt}^B .

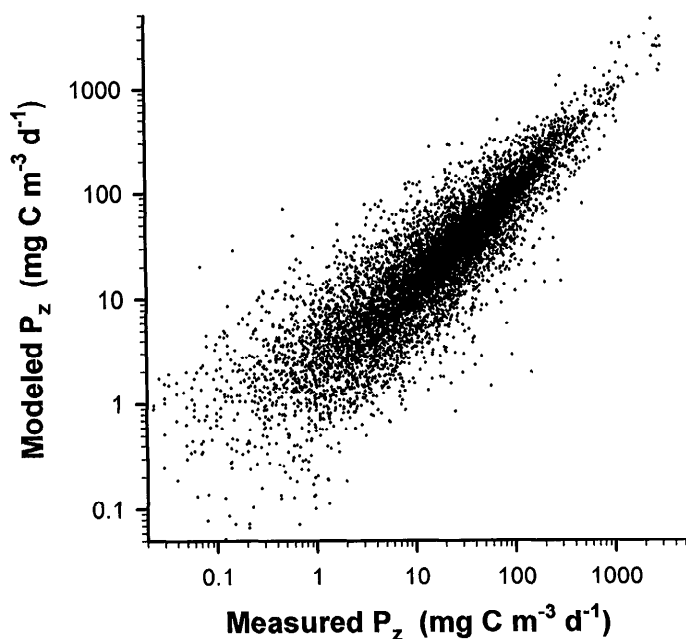


Fig. 4. Comparison of depth-resolved modeled primary production with measurement values for each sample depth (P_z , $mg C m^{-3} d^{-1}$) ($r^2 = 0.78$, $n = 10,857$). Not included in this comparison are measurement data from productivity profiles with $P_{opt}^B > 20 mg C (mg Chl)^{-1} h^{-1}$ (see discussion), which represented 4.6% of the MARMAP data (i.e. 48 profiles) and 0.9% of all other data (i.e. 6 profiles).

= 1,041), the VGPM accounted for 58% of the observed variability in PP_{eu} when P_{opt}^B was estimated with Eq. 11 (53% for \log_{10} -transformed data) (Fig. 8), which is a considerable improvement over a $C_{z0} \times Z_{cu}$ -type model or a Ψ -type (i.e. $C_{z0} \times Z_{cu} \times E_0$) model (see above). However, for the same reduced dataset, the VGPM explains 80% of the variability in PP_{eu} using measured values of P_{opt}^B (87% for \log_{10} -transformed data), illustrating that enhanced model performance remains dependent upon improvements in the P_{opt}^B model.

Discussion

Our purpose was to evaluate the importance of highly resolved vertical characterization of euphotic zone productivity and to identify the predominant factor(s) responsible for observed variability in depth-integrated primary production (PP_{eu}). We found that once euphotic depth (Z_{cu}), chlorophyll concentration (C_z), and photoperiod (D_{irr}) were accounted for, variability in the relative vertical distribution of primary production could be adequately modeled with a simple formulation consisting of a highly constrained, light-limited slope and a variable, light-dependent photoinhibition term. The generic vertical profiles generated by this simple formulation accounted for 86% of the observed variability in PP_{eu} when scaled to measured optimal assimilation efficiencies (P_{opt}^B). Our VGPM accounts for the relative light-saturated fraction of the euphotic zone as a function of surface PAR (E_0), but requires estimates of far fewer input variables than do the bio-optical models. Additionally, we found that inclusion of estimated C_z profiles did not improve model performance, thereby permitting reduction of the VGPM to a single equation relating PP_{eu} to C_{sat} , Z_{cu} , D_{irr} , P_{opt}^B , and E_0 . Thus, our

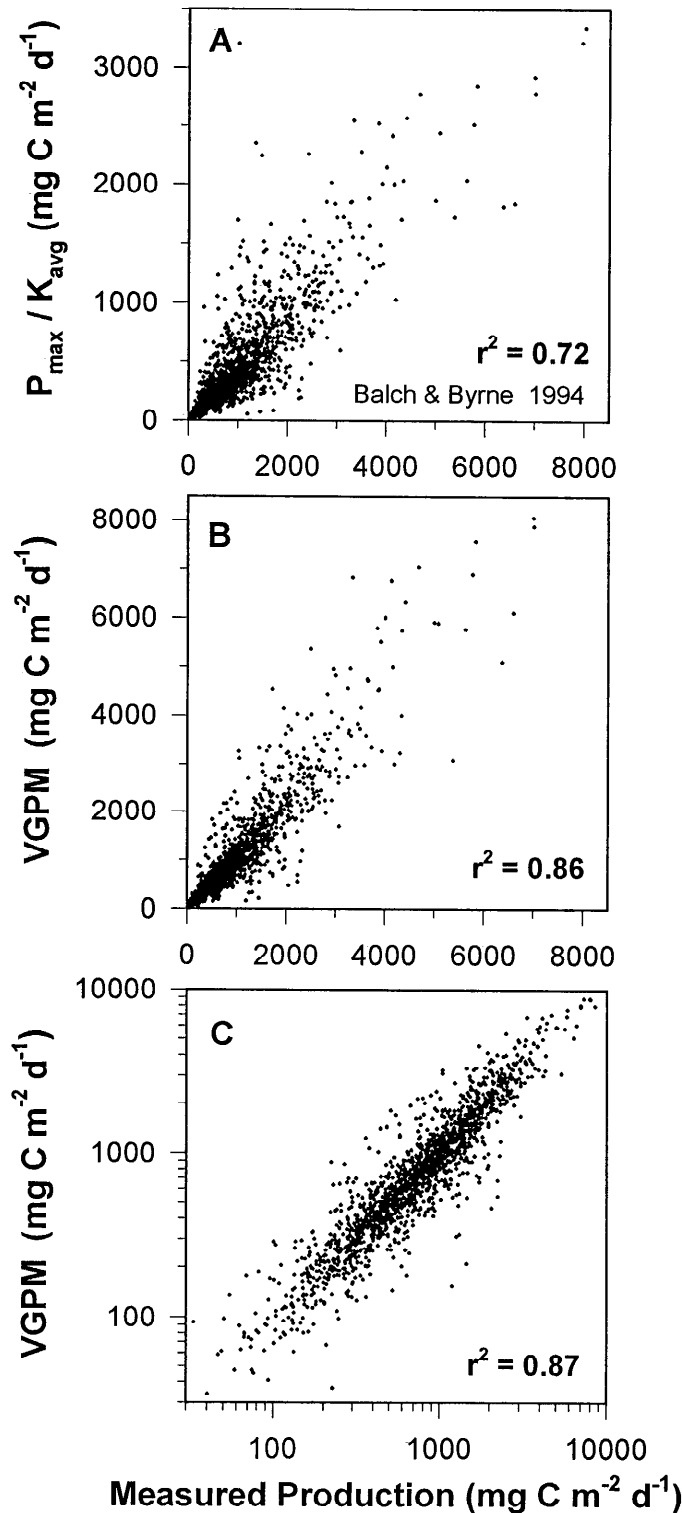


Fig. 5. Comparison of measured and modeled daily depth-integrated primary production (PP_{eu}) from measured values for the photoadaptive parameters, P_{\max} or P_{opt}^B , and (A) the P_{\max}/K_{avg} model of Balch and Byrne (1994) ($r^2 = 0.72$) and (B,C) the simplified VGPM (Eq. 10) where panel B is the normal axis ($r^2 = 0.86$) and panel C is the logarithmic transformation ($r^2 = 0.87$). Improved performance of the VGPM over the P_{\max}/K_{avg} model results primar-

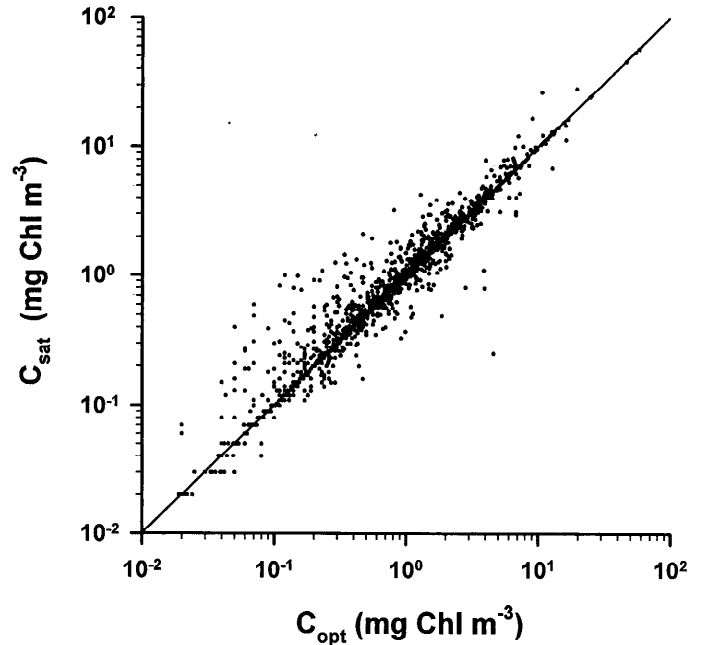


Fig. 6. Relationship between chlorophyll concentration at P_{opt}^B (i.e. C_{opt}) and surface chlorophyll (C_{sat}) for all 1,698 observations ($r^2 = 0.94$). Solid line indicates 1:1 correlation.

results illustrate that productivity algorithm performance in estimating PP_{eu} is critically dependent on the ability to accurately represent *spatial* (i.e. horizontal) and *temporal* variability in P_{opt}^B , not vertical variability in P_z .

The predominant influence of P_{opt}^B on model performance implies that, given identical fields of chlorophyll, irradiance, and euphotic depth, differences between productivity algorithms in reproducing measured values of PP_{eu} can be attributed primarily to differences in P_{opt}^B estimates. Diverse methods exist for estimating P_{opt}^B , ranging from direct (e.g. Eq. 11) and indirect (e.g. as a byproduct of establishing parameters for α , P_{\max}^B , β ; Morel 1991) formulations to categorization of oceanic biogeographical provinces (Longhurst et al. 1995). In the following sections, we discuss different methods for estimating P_{opt}^B or P_{\max}^B , estimate seasonal and annual global primary production using the VGPM and C_{sat} images from the CZCS to illustrate the effect of our P_{opt}^B model (Eq. 11) on geographical distributions of production, compare our estimates of global primary production with previously published estimates for oceanic and terrestrial systems, and discuss approaches for improving algorithm performance.

Estimates of P_{opt}^B and P_{\max}^B —Spatial variability in P_{opt}^B is influenced predominantly by variability in P_{\max}^B . Platt and coworkers (Platt and Sathyendranath 1988; Platt et al. 1991, 1992; Sathyendranath and Platt 1993; Longhurst et al. 1995)

←

ily from the irradiance-dependent VGPM function described by Eq. 9. $n = 1,693$ for all comparisons.

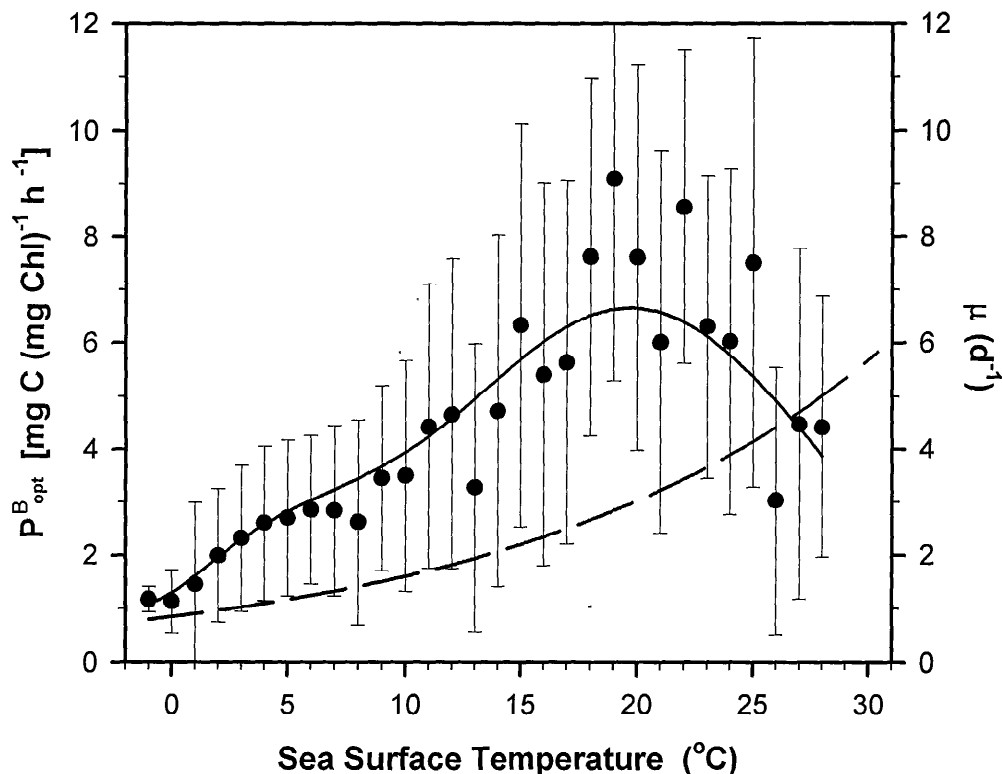


Fig. 7. Measured (●; \pm SD) and modeled (—; Eq. 11) median value of the photoadaptive parameter, P_{opt}^B , as a function of sea surface temperature. Dashed curve indicates the theoretical maximum specific growth rate (μ ; d^{-1}) of photoautotrophic unicellular algae described by Eppley (1972), which is used in a variety of productivity models (e.g. Balch and Byrne 1994; Antoine et al. 1996).

have established parameters for spatial variability in P_{max}^B by defining biogeographical provinces with consistent photosynthesis–irradiance (P vs. E) characteristics. Such an approach is hindered by the lack of sufficient data to fully characterize variability within each of the >50 provinces identified by Longhurst et al. (1995). Predictive capacity of provincially based models is also limited when boundaries are defined geographically because natural environmental variability ensures that these boundaries will not be static over time, particularly if predicted changes in global climate alter the frequency of wind-forced mixing events or ocean circulation patterns (Manabe and Wetherald 1974). Thus, efforts have been made to relate provincial boundaries to remotely sensed environmental variables, such as sea surface temperature (Platt et al. 1992; Sathyendranath and Platt 1993).

An alternative approach to provincial mapping of P vs. E variables is to identify principal environmental factors governing spatial variability in P_{opt}^B and then develop a series of equations and parameters for these relationships. SST has been a primary environmental variable used for developing such relationships because enzymatically controlled rate processes, such as P_{max}^B or P_{opt}^B , should exhibit temperature-dependence and because SST can be detected remotely. Unfortunately, research investigating relationships between temperature and algal metabolism in the adapted state has

previously focused more on specific growth rates (μ) than on photosynthesis (Jørgensen 1968; Eppley 1972; Li 1980). By consolidating independent results from numerous such studies, Eppley (1972) described a positive exponential relationship ($Q_{10} = 1.88$) between maximum attainable μ and temperature (Fig. 7). The model described by Eppley (1972) has subsequently been incorporated into primary productivity algorithms, such as the bio-optical model developed at the LPCM (Morel 1991; Antoine et al. 1996) that varies P_{max}^B as a function of the temperature-dependent variable KPUR ($1 \leq P_{max}^B \leq 6$ for $1^\circ C \leq T \leq 29^\circ C$).

The VGPM uses Eq. 11 to describe the observed increase in P_{opt}^B between -1 and $20^\circ C$ and subsequent decrease at temperatures $>20^\circ C$. Three fundamental differences exist between the temperature-dependent relationship described by Eppley (1972) and our P_{opt}^B model. First, the Eppley relationship was developed for μ and the P_{opt}^B model for photosynthesis, with different responses between μ and P_{opt}^B being related to direct and indirect effects of temperature on C:Chl ratios (Davison 1991; Maxwell et al. 1995; Geider et al. 1996). Second, the curve described by Eppley increases exponentially from -1 to $29^\circ C$, whereas the model for P_{opt}^B decreases above $20^\circ C$ (Fig. 7). Finally, Eppley's curve describes a *maximum envelope* for μ , whereas the P_{opt}^B model describes a *median*.

The P_{opt}^B model also differs from the relationship used by

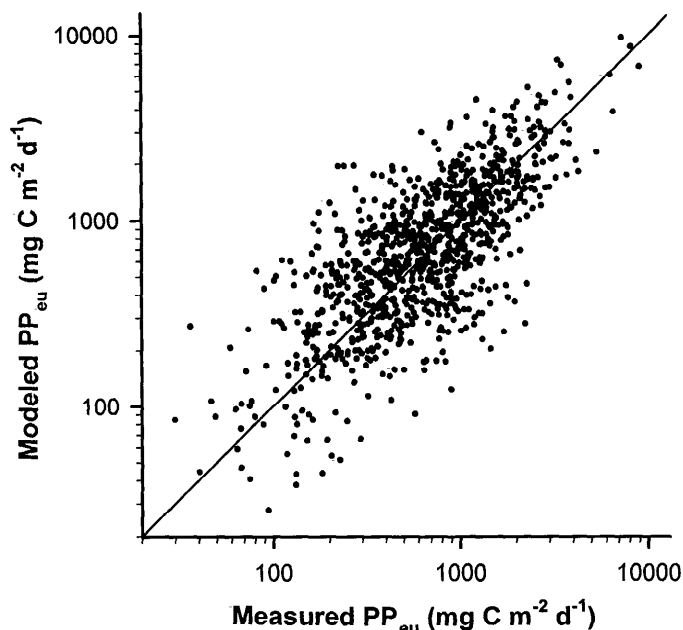


Fig. 8. Relationship between measured and modeled daily depth-integrated primary production (PP_{eu}), where VGPM estimates are based on P_{opt}^B values calculated by means of sea surface temperatures and Eq. 11 ($r^2 = 0.58$; $n = 1,013$). Measured productivity profiles with $P_{opt}^B > 20$ mg C (mg Chl) $^{-1}$ h $^{-1}$ were excluded from this comparison (see discussion). Solid line indicates 1:1 correlation.

Balch et al. (1992) for comparisons between empirical productivity models and the bio-optical model of Platt and Satyendranath (1988), where P^B (their correlative to $P_{opt}^B \times \int_0^z C_2$) was described as a negative exponential function of temperature. In a subsequent report, Balch and Byrne (1994) described P_{max}^B as a function of SST and a Michaelis-Menten relationship between μ and NO_3^- concentration, but again this two-factor model for P_{max}^B describes a maximum envelope and the P_{opt}^B model describes a median. Finally, although common features exist between our P_{opt}^B model and the shape of Arrhenius curves for algal photosynthesis, these functions differ because SSTs used in the P_{opt}^B model represent growth temperatures (Sakshaug et al. 1989; Cullen 1990), whereas Arrhenius curves describe tolerances over a range of assay temperatures for phytoplankton from a single growth temperature (Li 1980). In fact, within the relevant range of SST, algal photosynthesis in the adapted state should not be directly inhibited by increasing growth temperatures (Li 1980). Observed decreases in P_{opt}^B above 20°C must therefore be attributed to other factors associated with regions of elevated SST.

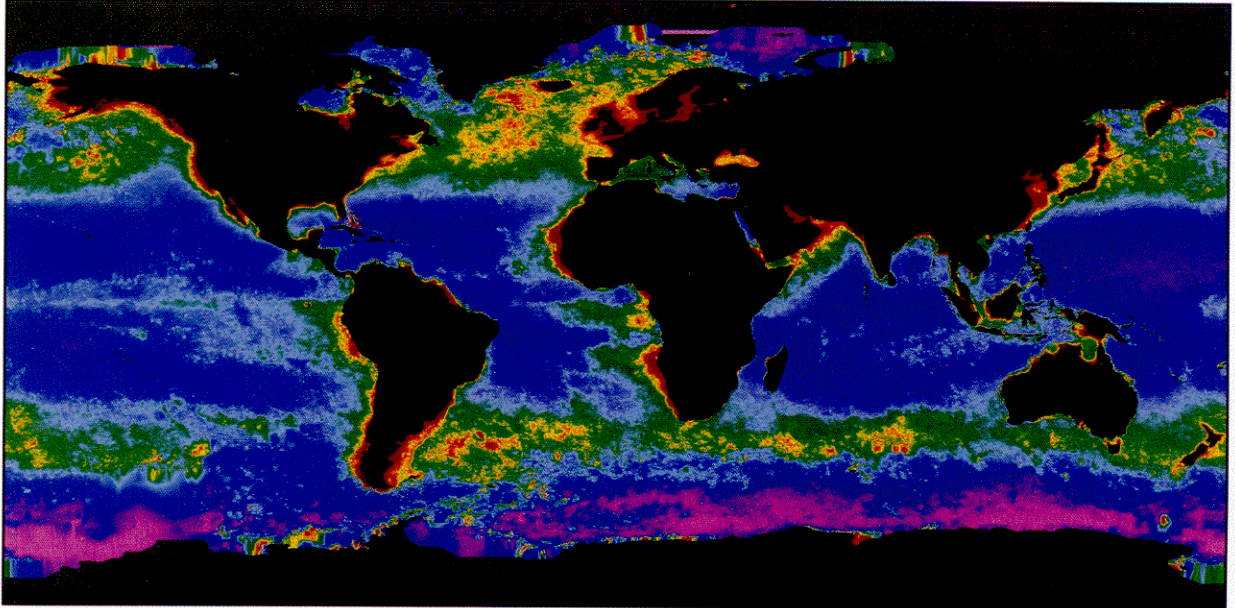
Unexplained variance in P_{opt}^B and disparity between temperature-dependent functions used in productivity models indicate that much work remains before P_{opt}^B is properly characterized. Although temperature alone will not be sufficient to adequately model P_{opt}^B , it is clear that temperature is an important factor regulating spatial variability in P_{opt}^B , which has the following implications regarding global oceanic primary production:

- Variability in SST occurs at spatial and temporal scales far smaller than the limit imposed on the characterization of biogeographic provinces by the availability of ^{14}C -uptake measurements and thus compromises such an approach for establishing parameters for P_{opt}^B models.
- Large-scale oceanic primary production is critically linked to SST and thus is acutely susceptible to alterations due to current changes in radiatively important atmospheric gas concentrations.
- Although chlorophyll concentration (an indicator of biomass) alone may prove a sufficient indicator of change in global productivity, it will not provide an accurate estimate in the absolute change in carbon fixation (a measure of biological rate) because the ratio of chlorophyll per unit carbon fixed is nonlinearly temperature-dependent.

VGPM estimates of oceanic carbon fixation—We calculated global annual phytoplankton carbon fixation (PP_{annu}) to illustrate the importance of temperature-dependent variability in P_{opt}^B on the geographical distribution of PP_{annu} and to compare VGPM results with PP_{annu} calculations from other models. VGPM estimates of PP_{annu} were made with monthly climatological averages (1978–1983) of global C_{sat} , as measured by the CZCS on the Nimbus-7 satellite. P_{opt}^B was modeled with Eq. 11 and monthly climatological average SST was derived from shipboard measurements and archived in the U.S. Navy Marine Climatic Atlas. Climatological monthly average E_0 during the CZCS period, corrected for cloudiness, was provided by the NCAR data archives (Bishop and Rossow 1991). Euphotic depths were calculated according to Morel and Berthon (1989). Seasonal and annual global production was calculated by integrating the VGPM monthly estimates of PP_{eu} . We assume that the contribution of pheopigments to C_{sat} is negligible (Claustre and Marty 1995) and equate C_{sat} to total active chlorophyll. For comparative purposes, we also calculated PP_{annu} by using a constant value for P_{opt}^B of 4.54 mg C (mg Chl) $^{-1}$ d $^{-1}$ (the median value of P_{opt}^B from our productivity dataset) and an exponential model for P_{opt}^B following Eppley (1972) and normalized to 4.6 mg C (mg Chl) $^{-1}$ d $^{-1}$ at 20°C to permit direct comparison with LPCM results (Antoine et al. 1996).

The VGPM estimate of PP_{annu} with Eq. 11 for P_{opt}^B was 43.5 Pg C yr $^{-1}$ (i.e. petagrams C yr $^{-1}$ = Gt C yr $^{-1}$) (Fig. 9A). A constant value for P_{opt}^B increased PP_{annu} by 7% to 46.5 Pg C yr $^{-1}$. Replacing Eq. 11 in the VGPM by the normalized exponential function of Eppley (1972) resulted in an estimate for PP_{annu} of 42.9 Pg C yr $^{-1}$ (Fig. 9B), which is not only close to the LPCM estimate of 45.6 Pg C yr $^{-1}$ but is also similar in its geographical distribution (cf. our Fig. 9B with figure 3 of Antoine et al. 1996). All three models for P_{opt}^B resulted in distinctly different relative distributions of PP_{annu} . From the perspective of modeling biogeochemical carbon cycles, these geographical differences are at least as important as the total carbon fixed because differences in the physical and biological characteristics of water masses influence the fractionation of biologically fixed carbon into that which is rapidly respired within the euphotic zone and that which is ultimately removed from the surface layer to rep-

A



B

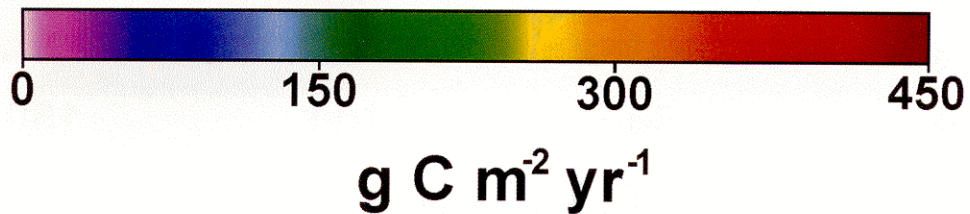
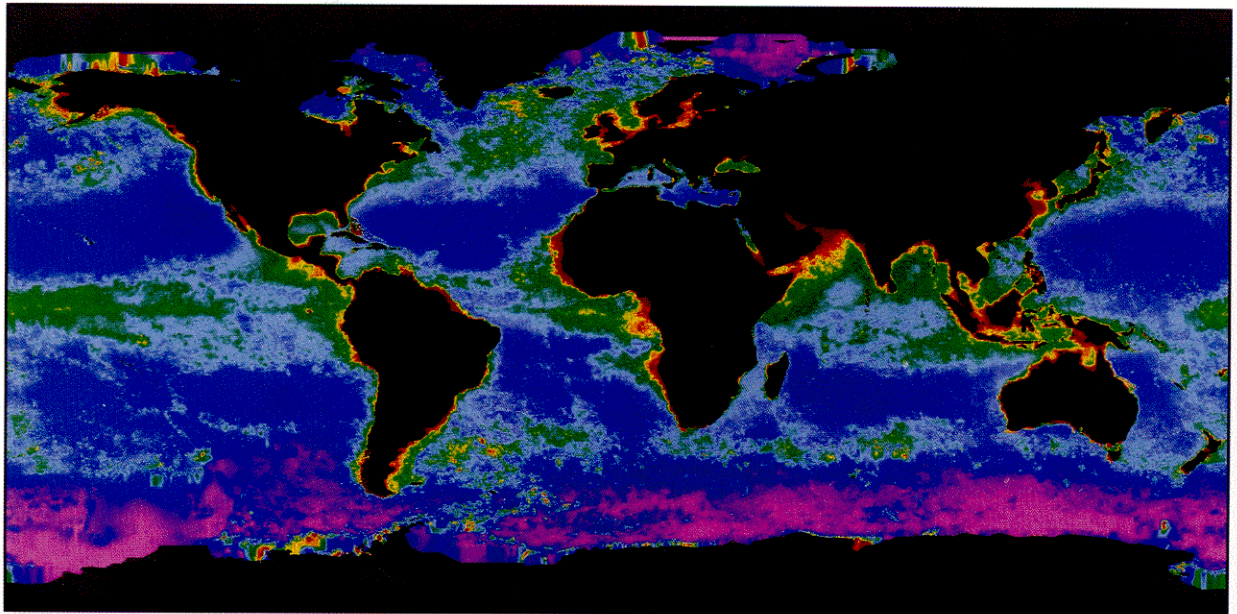
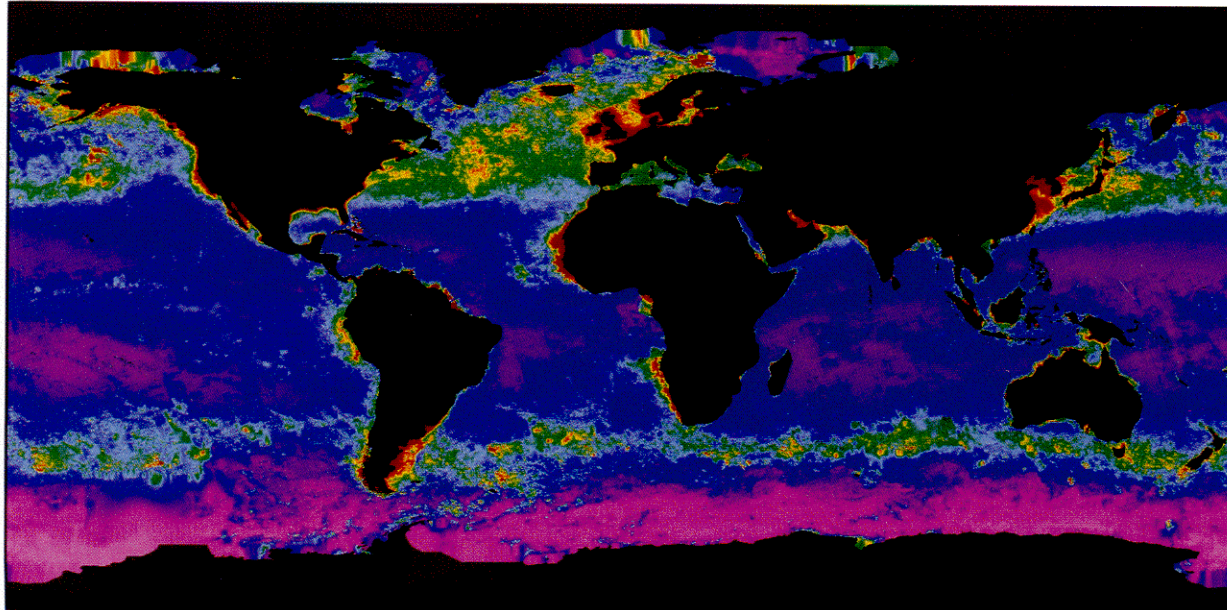
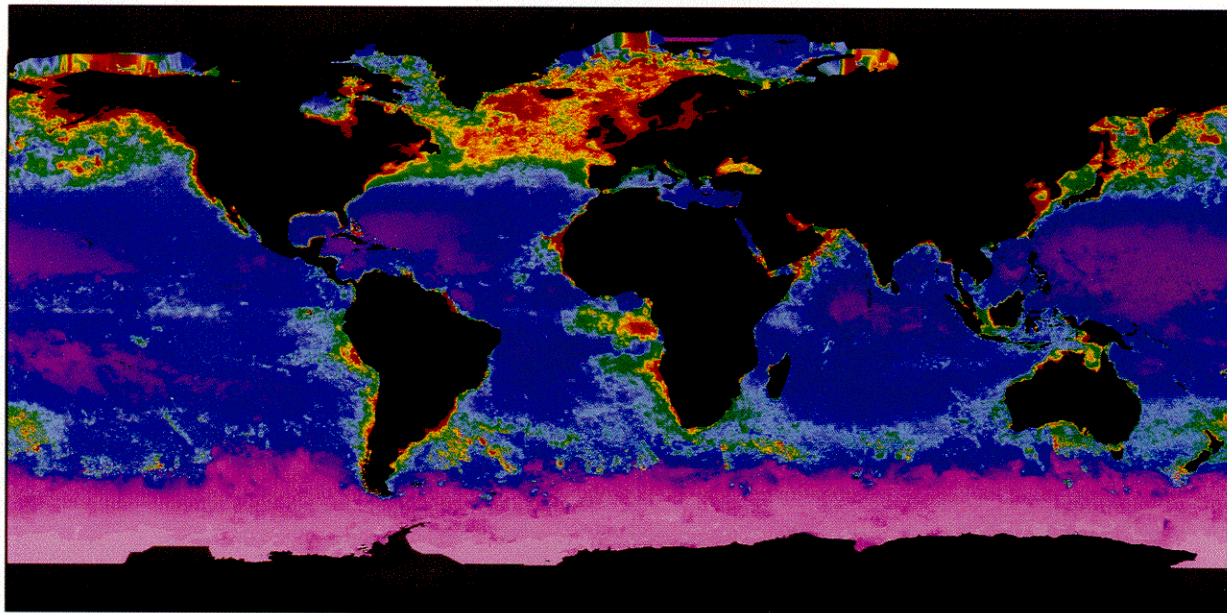


Fig. 9. Global estimates of annual (PP_{annu}) and seasonal (PP_{season}) phytoplankton primary production using the VGPM, climatological monthly mean CZCS C_{sat} , sea surface temperature, and cloudiness-corrected surface irradiance. A. PP_{annu} calculated with the temperature-dependent model for P_{opt}^B described by Eq. 11. B. PP_{annu} calculated as in panel A but with the exponential temperature-dependent model of Eppley (1972) normalized to $4.6 \text{ mg C (mg Chl)}^{-1} \text{ h}^{-1}$ at 20°C , as by Antoine et al. (1996).

C



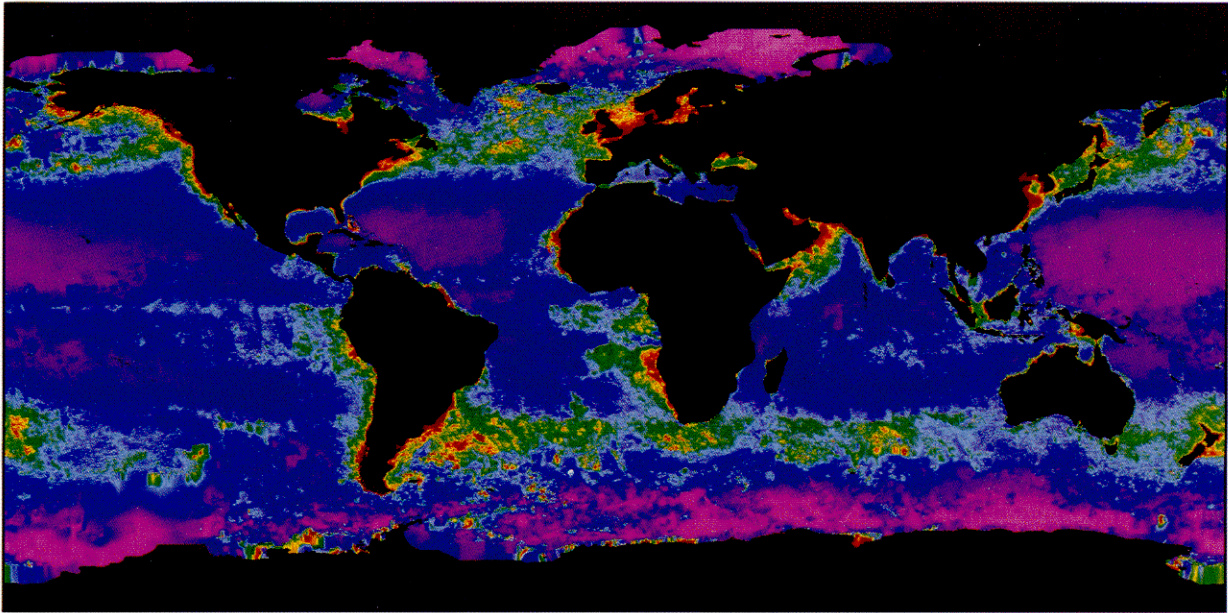
D



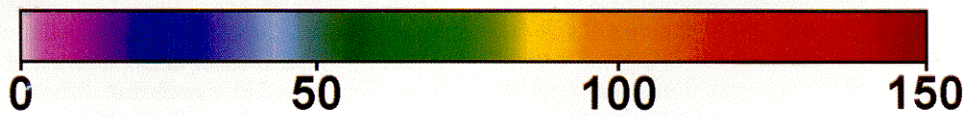
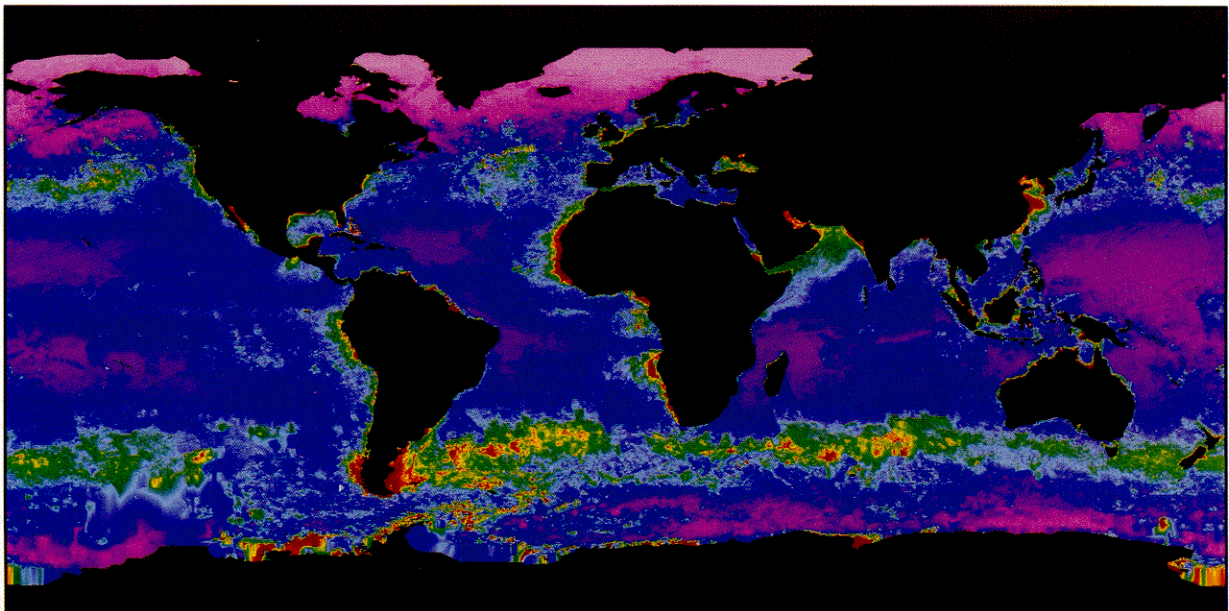
g C m⁻² season⁻¹

Fig. 9 (contd). C-F. PP_{season} calculated with the P_{opt}^{β} model described by Eq. 11 for March-May (C), June-August (D), September-November (E), and December-February (F).

E



F



g C m⁻² season⁻¹

Fig. 9 (contd).

resent a net loss of carbon from the atmosphere (Walsh 1984; Bakun 1990; Wirick 1994).

The distribution of PP_{annu} calculated with a constant P^B_{opt} differed from results with the temperature-dependent functions because of geophysical phenomena controlling global SST distributions. For example, a constant value for P^B_{opt} resulted in a relatively uniform distribution of productivity across the northern North Atlantic. In contrast, productivity calculated with Eq. 11 was considerably lower along the western margin of the northern North Atlantic than in the central and eastern regions because of a tongue of cooler waters descending from the north along the northeastern boundary of North America (Thurman 1985). Along the Gabon coast of western Africa, Eq. 11 resulted in enhanced estimates of production compared to results for a constant P^B_{opt} and lower values compared to the exponential model (cf. Fig. 9A and B) owing to the warmer, more stratified water mass in the offshore reaches of this region.

Results for the three P^B_{opt} models were particularly divergent in regard to production within the central ocean gyres and the Southern Ocean. Compared to the exponential model, Eq. 11 resulted in a more pronounced gradient in primary production within the central ocean gyres, particularly in the western boundary of the tropical Pacific where wind-driven net transport of warm surface waters during non-ENSO years results in unusually deep thermoclines, extreme nutrient depletion in the euphotic zone, and high mixed-layer water temperatures (a region commonly referred to as the Western Pacific Warm Pool) (Thurman 1985; Lindstrom et al. 1987). Use of Eq. 11 also resulted in lower production values along the equatorial upwelling belts (Fig. 9A,B). Finally, estimates of annual Southern Ocean productivity were greatest for the constant P^B_{opt} model and lowest for the exponential model (Fig. 9B), whereas use of Eq. 11 resulted in a moderate estimate for production in this region that was restricted primarily to the Antarctic Convergence (Fig. 9A).

Seasonal global primary production (PP_{season}) was remarkably consistent throughout the year, ranging from 10.4 Pg C in winter (December–February) to 11.5 Pg C in summer (June–August). The distribution of PP_{season} , however, varied greatly (Fig. 9C–F). Extensive phytoplankton blooms in the North Atlantic and continental shelf regions of the North Pacific caused global PP_{season} to be greatest in spring (March–May) (Fig. 9C) and summer (Fig. 9D), despite considerable blooms in the region of the Antarctic Convergence during autumn (September–November) (Fig. 9E) and winter (Fig. 9F). As anticipated, irradiance (E_0) had a prominent influence on PP_{season} distributions, which is best illustrated during summer (Fig. 9D) and winter (Fig. 9F) months. A result that was not anticipated, however, was that removing the influence of cloudiness on E_0 (i.e. running the VGPM for clear sky conditions) increased PP_{annu} by only 3.4% (i.e. to 45.0 Pg C yr⁻¹). This nominal effect of cloudiness is attributed to the opposing effects of surface photoinhibition and light-limitation at depth. Explicitly, estimates of PP_{eu} become relatively irradiance-insensitive as E_0 exceeds ~ 20 mol quanta m⁻² d⁻¹ because potential increases in PP_{eu} resulting from a deepening of the light-saturated region of the euphotic zone as E_0 increases are offset by the simultaneous increases in

surface photoinhibition (however, see modeling photoinhibition below).

Intermodel comparisons of oceanic production—We have discussed a few of the many differences between productivity models. To see how these differences affect estimates of PP_{annu} , we compared the VGPM calculations with published results from the LPCM (Antoine et al. 1996), the Bedford Institute of Oceanography (BPM) (Longhurst et al. 1995) bio-optical models, and a compilation by Eppeley and Peterson (1979) (E&P) based on calculations by Platt and Subba Rao (1975). The VGPM estimate of 43.5 Pg C yr⁻¹ for PP_{annu} is only slightly lower than the LPCM (46.9 Pg C yr⁻¹) and BPM (50.2 Pg C yr⁻¹) estimates and is considerably higher than the E&P estimate of 27.1 Pg C yr⁻¹, which was based on rough estimates of global chlorophyll concentration and is generally considered an underestimate of PP_{annu} .

Similarities and discrepancies between model estimates of PP_{annu} are better illustrated by comparing geographical distributions of PP_{annu} . We used the five geographical divisions (Pacific, Atlantic, Indian, Arctic, Antarctic) defined by Antoine et al. (1996) to compare basin-scale distributions of PP_{annu} for the VGPM, LPCM, and BPM models (Table 2). For this comparison, BPM production estimates for each basin were recalculated from Longhurst et al. (1995) by summing provincial production values located within the geographical boundaries defined by Antoine et al. (1996). Thus, BPM values in Table 2 for each ocean basin differ slightly from values reported by Longhurst et al. (1995). Basin-scale production values for the E&P model are exactly as published by Eppeley and Peterson (1979) and are included for first-order comparisons only, since these boundaries differ from Antoine et al. (1996). Distributions of PP_{annu} were compared further for the VGPM and LPCM models by using the three trophic categories defined by Antoine et al. (1996) based on annual average C_{sat} , namely oligotrophic ($C_{\text{sat}} \leq 0.1$ mg Chl m⁻³), mesotrophic ($0.1 < C_{\text{sat}} \leq 1.0$ mg Chl m⁻³), and eutrophic ($C_{\text{sat}} > 1.0$ mg Chl m⁻³).

Although methods for estimating critical photoadaptive parameters differed most between the VGPM and BPM, these two models exhibited the greatest similarity when relative basin scale distributions of PP_{annu} were compared (Table 2). The VGPM and BPM were particularly similar in the percentages of PP_{annu} assigned to the Pacific, Atlantic, and Indian Ocean basins and differed primarily in their estimates of polar production. In contrast, the LPCM assigned a significantly larger fraction of PP_{annu} to the Pacific and Indian Ocean basins and lower fraction to the Antarctic basin than did the VGPM or BPM. The relative contribution of the Atlantic basin to PP_{annu} , however, was remarkably consistent for all three models and was even similar for the E&P estimate. Comparison of the VGPM and LPCM on a trophic basis also revealed significant differences between modeled distributions of PP_{annu} . The LPCM assigned a relatively large contribution of PP_{annu} to oligotrophic regions, whereas the VGPM results indicated much lower oligotrophic than mesotrophic production. This discrepancy between trophic production estimates can be traced directly to the different temperature-dependent functions used in the two models for P^B_{opt} and P^B_{max} . The positive exponential temperature function

Table 2. Global annual phytoplankton primary production (Pg C yr⁻¹) calculated with the vertically generalized production model (VGPM), Laboratoire de Physique et Chimie Marines (LPCM) model (Antoine et al. 1996), Bedford production model (BPM) (Longhurst et al. 1995), and the Eppley and Peterson (1979) compilation (E&P). Annual production is also shown for the five major ocean basins defined by Antoine et al. (1996) (percentages of total production indicated in parentheses), as well as three trophic categories for the VGPM and LPCM models (subpolar plus global in brackets).

	VGPM	LPCM*	BPM†	E&P‡
Global total	43.5	46.9	50.2 _{44.7} ^{46.3}	27.1
Pacific	16.7(38.3)	20.0(42.7)	19.4 _{17.4} ^{18.1} (38.6)	9.1(33.7)
Atlantic§	11.9(27.5)	11.3(24.0)	13.7 _{10.8} ^{11.7} (27.3)	8.6(31.6)
Indian	6.2(14.2)	8.1(17.3)	6.5 _{6.0} ^{6.2} (13.0)	6.0(22.0)
Arctic	0.4(0.9)	0.6(1.3)	1.4(2.8)	0.1(0.5)
Antarctic	8.3(19.1)	6.9(14.7)	9.2(18.3)	3.3(12.2)
Oligotrophic	10.3[10.5]	16.2		
Mesotrophic	22.0[26.4]	22.5		
Eutrophic	3.6[6.6]	2.5		

* All LPCM production values are for model results when the contribution of pheopigments to C_{sat} is negligible. LPCM production values were recalculated by D. Antoine with the identical CZCS pigment data used for the VGPM calculations and thus differ slightly from results reported by Antoine et al. (1996).

† Annual production values for the BPM calculated with standard values for model variables are indicated by the larger numbers. The superscript and subscript values are annual production estimates when nonalgal particles in turbid coastal waters reduce the active chlorophyll component of water-leaving radiance by 50% and 75%, respectively.

‡ Division of annual production into the primary ocean basins is taken directly from Eppley and Peterson (1979) and may not correspond exactly to divisions described by Antoine et al. (1996).

§ Annual production for the Mediterranean Sea is included in Atlantic ocean production.

|| The three trophic categories were defined using annual average C_{sat} as oligotrophic— $C_{\text{sat}} \leq 0.1 \text{ mg m}^{-3}$; mesotrophic— $0.1 < C_{\text{sat}} \leq 1 \text{ mg m}^{-3}$; and eutrophic— $C_{\text{sat}} > 1 \text{ mg m}^{-3}$ (Antoine et al. 1996). Trophic productivity was reported by Antoine et al. (1996) for latitudes between 50°N and 50°S. For comparison, trophic production values for the VGPM are shown for the same latitudinal band, but global values (90°N–90°S) are included in brackets.

used in the LPCM results in higher relative carbon fixation per unit chlorophyll in warmer oligotrophic regions than in cooler mesotrophic regions, whereas the VGPM associates warmer regions with higher nutrient stress and suppressed P^B_{opt} . These differences in PP_{annu} distributions are particularly critical if models of oceanic carbon fixation are used in global climate models for estimating the ocean–atmosphere CO₂ exchange because the fraction of total fixed carbon representing new production differs between oligotrophic, mesotrophic, and eutrophic regions (Eppley and Peterson 1979).

Functioning of the oceans in the biosphere—Model estimates of global PP_{annu} (e.g. Table 2) can be used to examine the efficiency of the photoautotrophic biomass in the oceans relative to the available energy impinging upon the system or in comparison to efficiencies for terrestrial systems. For comparative purposes, we elaborate here on calculations of ecosystem functioning previously reported by Antoine et al. (1996). From a purely energetic viewpoint, the efficiency of the oceans' plant biomass can be evaluated from the ratio of photosynthetically stored radiation (PSR) to photosynthetically available radiation (PAR) (Morel 1978). The global PP_{annu} of 43.5 Pg C yr⁻¹ calculated with the VGPM is roughly equivalent to $1.7 \times 10^{18} \text{ kJ yr}^{-1}$ PSR [assuming an average conversion of 39 kJ gC⁻¹ as described by Morel (1991)]. PAR over the oceans, including the correction for cloudiness, averaged $4.49 \times 10^{18} \text{ mol quanta yr}^{-1}$ during the CZCS period, which is equivalent to $9.76 \times 10^{20} \text{ kJ yr}^{-1}$ PAR

[using the factor $2.77 \times 10^{21} \text{ quanta s}^{-1} \text{ kW}^{-1}$ for the solar PAR spectrum from Morel and Smith (1974)]. Thus, the ratio of PSR:PAR gives a global average efficiency of 0.17% for the conversion of PAR into photosynthetically fixed organic carbon, which is slightly higher than the value of 0.13% calculated by Morel (1991).

From a biophysical viewpoint, it is often more useful to assess the photon requirement or yield of the oceans' biomass, as opposed to the energetic efficiency, because excitons arriving at photosynthetic reaction centers are equally effective in causing primary charge separation, regardless of the energy (i.e. wavelength) of the absorbed photon. Photon yield is easily calculated as the ratio of annually available moles of photosynthetically active photons to annually fixed moles of carbon, which gives an average of 1,250 photons incident on the sea surface per fixed carbon atom.

A similar calculation can be made for the terrestrial plant biomass using a net global annual carbon fixation rate of between 50 and 65 Pg C yr⁻¹ (Lurin et al. 1994). The global annual photon flux over land is $\sim 2 \times 10^{18} \text{ mol quanta yr}^{-1}$, giving a terrestrial photon efficiency of ~ 375 –500 photons per atom of carbon fixed. Thus, the terrestrial component of the biosphere is ~ 2.9 times more effective at harvesting the available solar radiation than is the oceanic component, as would be expected because the marine biomass must compete with its strongly absorbing medium for light.

The global annual average C_{sat} of 0.28 mg Chl m⁻³ can be used to compare biomass-specific rates between oceanic

and terrestrial systems. From Morel and Berthon (1989), a C_{sat} of 0.28 mg Chl m^{-3} would correspond to an average Z_{eu} of 56 m and a depth-integrated chlorophyll concentration (C_{cu}) of 22 mg Chl m^{-2} . Combining C_{cu} and the photon efficiency [i.e. (mol C/mol photons) \times (1/ C_{cu})] results in a global average estimate of 0.44 for the biomass-specific efficiency (Ψ) of the oceans, nearly identical to the original estimate of 0.43 for Ψ (Falkowski 1981). Assuming a C:Chl ratio ranging from 40 to 100 g C (g Chl) $^{-1}$, the carbon biomass of the oceans (area = 3.39×10^{14} m^2) is between 0.30 and 0.75 Pg. With an annual budget of 43.5 Pg C yr^{-1} , the average turnover time of the oceans' biomass is 2–6 d. In a similar manner, turnover time of the terrestrial plant biomass was calculated as 13–16 yr (total biomass = 800 Pg C; total area = 1.43×10^{14} m^2). Thus, compared to the terrestrial system, the greatly reduced biomass and rapid turnover time in the oceans implies a much lower capacity for long-term carbon storage, unless a rapid mechanism for sequestering fixed carbon and replenishing utilized nutrients can be identified (Sarmiento et al. 1992; Sarmiento and Siegenthaler 1992; Falkowski 1994).

Improving the VGPM—Uncertainties in our global estimates of PP_{cu} can be subdivided into errors associated with each of the five variables required by the VGPM, namely P_{opt}^B , E_0 , Z_{cu} , C_{opt} , and D_{irr} . Photoperiod (D_{irr}) is calculated exactly and thus does not contribute errors to PP_{cu} estimates. Daily surface PAR (E_0) calculated for clear sky conditions and corrected for cloudiness has an estimated error of <5% and, when considered in conjunction with the insensitivity of VGPM estimates to E_0 changes above ~ 20 mol quanta $\text{m}^{-2} \text{d}^{-1}$, indicates that model errors in E_0 will have a negligible effect on global estimates of PP_{cu} . Calculations of Z_{cu} based on C_{sat} are less precise than E_0 estimates and have associated errors of <15% in case 1 waters (Morel and Prieur 1977; Morel 1988; Morel and Berthon 1989). In case 2 waters (Morel and Prieur 1977), errors in C_{sat} -based calculations of Z_{cu} are considerably larger (Kirk 1994), although improvements in remote sensing algorithms for these regions are progressing. Nevertheless, errors in PP_{cu} resulting from Z_{cu} estimates are of secondary importance compared to errors associated with C_{opt} and P_{opt}^B .

The predominant source of error in C_{opt} does not result from equating C_{opt} to C_{sat} (estimated error of <5%), but rather from extracting C_{sat} from remotely sensed measurements of water-leaving radiance. CZCS satellite-pigment algorithms (Clarke et al. 1970; Gordon and Clark 1980a,b, 1981; Gordon et al. 1983) gave overall accuracies in phytoplankton pigment (Chl *a* + pheopigment) of ± 0.3 log units (Gordon et al. 1983; Balch et al. 1992). Improvements in satellite ocean color sensor optics and calibration, along with an increase in the number of wavebands available for pigment detection, will decrease the error in future C_{sat} estimates. C_{sat} errors are common to all productivity models and thus do not contribute to model difference in the derivation of biological rates (i.e. PP_{cu}) from measurements of biomass (i.e. C_{sat}).

The largest errors in VGPM estimates of PP_{cu} are associated with calculations of P_{opt}^B . Less than half of the observed variability in P_{opt}^B is explained by our temperature-

dependent model (Eq. 11). Although we attempted to assemble a methodologically consistent dataset, a portion of the unexplained variance in P_{opt}^B can still be attributed to factors such as differences in incubation durations, chlorophyll measurement techniques, and trace metal contamination (Fitzwater et al. 1982). Uncertain data quality also contributes to observed variability in P_{opt}^B , an issue that is difficult to evaluate objectively but cannot be ignored. An advantage of a dataset with $\sim 2,000$ stations is that we were able to visually inspect all 11,283 values for C_z and P_z . It soon became apparent from these inspections that the most influential data quality issue for our dataset, yet the most easily remedied in the field, was errors associated with measurements of chlorophyll. For example, Falkowski (1981) calculated that maximum light-saturated assimilation efficiencies should not greatly exceed 25 mg C (mg Chl) $^{-1} \text{h}^{-1}$ based on physiological constraints for oxygenic photosynthesis. Maximum values for P_{opt}^B should therefore be slightly lower due to photoinhibition at high E_0 and light-limitation near sunrise and sunset. Indeed, virtually all P_{opt}^B values > 20 mg C (mg Chl) $^{-1} \text{h}^{-1}$ and many values > 15 mg C (mg Chl) $^{-1} \text{h}^{-1}$ could be traced to anomalously low C_z values [note that P_{opt}^B exceeded 40 mg C (mg Chl) $^{-1} \text{h}^{-1}$ at 11 stations, one of which exceeded 100 mg C (mg Chl) $^{-1} \text{h}^{-1}$]. The anomalous C_z values were easily identified by the consistent values of C_z immediately above and below the anomalous sample and by the uniform P_z for all three depths. For example, in one of the profiles from our dataset, C_z and P_z measured at 3, 6, and 10 m had values of 0.22, 0.06, and 0.21 mg Chl m^{-3} and 12, 13, and 14 mg C $\text{m}^{-3} \text{d}^{-1}$. The anomalous C_z value (i.e. 0.06) resulted in a P_{opt}^B for the profile of 22 mg C (mg Chl) $^{-1} \text{h}^{-1}$, which clearly was not representative for the profile as a whole. C_z errors are more common than P_z errors because most investigators include at least three replicate bottles for measuring P_z , but typically only one sample is collected for C_z . This problem could be easily remedied by analyzing duplicate chlorophyll samples at each depth.

Although methodological inconsistencies and data quality issues contribute to variability in P_{opt}^B , much of the unexplained variance is due to physiological adjustments by phytoplankton to variable growth conditions that cannot be adequately accounted for by a single-factor P_{opt}^B model (e.g. Eq. 11). Because P_{opt}^B is the main variable controlling model performance and the variable with the greatest uncertainties, significant improvements in estimating oceanic primary production will not be forthcoming without considerable advances in our ability to predict temporal and spatial variability in P_{opt}^B . These improvements will require establishing parameters for multiple relationships between P_{opt}^B and various environmental factors and should focus on mechanistic, rather than statistical, relationships in order to foster enhanced predictive capacities of productivity algorithms.

As an initial approach, it may be advantageous to separate factors influencing P_{opt}^B into those affecting the normalization of P_{opt} to P_{opt}^B and those related to physiological processes regulating P_{opt} . Included in the former category are adaptive strategies related to changes in light quantity and spectral quality (Falkowski 1981, 1984; Falkowski and Owens 1980; Falkowski et al. 1981). Light spectra at E_{opt} vary as a function of suspended particulate (including phytoplank-

ton) and dissolved organic concentrations, whereas light quantity varies primarily as a function of solar angle and vertical mixing. Physiological adjustments to changes in light quality affect Chl:accessory pigment ratios and alter optical absorption cross sections (a^*) (Kirk 1994; Babin et al. 1996). Quantifying a relationship between a^* and P_{opt}^B could be particularly useful because upcoming ocean color sensors (e.g. SeaWiFS) will incorporate additional wavebands for evaluating accessory pigment concentrations. Light-shade adaptations to light quantity (Sakshaug and Andresen 1986; Berner et al. 1989; Sakshaug et al. 1989; Falkowski and LaRoche 1991) likely have greater effects on P_{opt}^B than does light quality, but establishing parameters for these responses in terms of remotely sensed variables will be more challenging than assessing spatial differences in a^* . One approach may be to couple mixed layer depth and wind stress estimates as an index of mean light exposure, since light-shade adaptations are affected by both the depth and rate of mixing (Cullen and Lewis 1988; Lande and Lewis 1989).

Mechanistic approaches will be particularly important for developing parameters for relationships between remotely sensed variables and factors regulating P_{opt} . Variability in P_{opt} is mainly due to variability in light-saturated photosynthetic rates (P_{max}). P_{max} can be equated to the cellular concentration of functional photosystem 2 reaction centers (n) and the electron turnover rate ($1/\tau$) of the photosynthetic light reactions (Falkowski 1980; Sukenik et al. 1987), where the product of n and $1/\tau$ under light-saturation is controlled by the concentration and activity of the Calvin cycle enzymes. From this physiological perspective, we can associate observed increases in P_{opt}^B between -1 and 20°C (Eq. 11) with changes in $1/\tau$ resulting from the direct effect of temperature on enzyme activity (assuming division by C_{opt} roughly accounts for changes in P_{opt} due to n). It is also clear that decreases in P_{opt}^B at $>20^\circ\text{C}$ are due to secondary factors associated with elevated SST, since the direct effect of temperature should cause $1/\tau$ to increase at $>20^\circ\text{C}$. Initially, we might speculate that decreases in P_{opt}^B at $>20^\circ\text{C}$ result from low nutrient concentrations coincident with high SST (Balch and Byrne 1994), since NO_3^- typically becomes undetectable at SST between ~ 15 and 20°C (Zentara and Kamykowski 1977; Kamykowski and Zentara 1986; Balch and Byrne 1994). However, the physiological effect of nutrient limitation is a simultaneous decrease in both n and $1/\tau$, resulting in only minor changes in P_{max}^B (Herzig and Falkowski 1989; Chalup and Laws 1990). It is more likely that decreases in P_{opt}^B observed at SST $>20^\circ\text{C}$ result from other factors associated with nutrient-impoverished oceanic regions, such as increased susceptibility to photoinhibition, larger respiratory rates, or changes in species composition (Geider and Platt 1986; Geider et al. 1986; Gallegos 1992).

The single-factor P_{opt}^B model presently used in the VGPM (Eq. 11) represents a statistical relationship that integrates a diversity of physiological phenomena into a simple temperature-dependent function. Improved VGPM performance requires transformation of this single, statistical P_{opt}^B function into multiple, mechanistic models (e.g. Balch and Byrne 1994) because relationships between SST and other factors

controlling variability in P_{opt}^B are not constant over space and time.

Modeling photoinhibition—In the preceding section we discuss the influence of errors associated with each of the VGPM variables on estimates of PP_{eu} . Errors in the photoinhibition (β_d) model (Eq. 5) also affect PP_{eu} , but are embedded within the irradiance-dependent function (Eq. 8). β_d decreases the quantum efficiency of photosynthesis in the upper water column, causing PP_{eu} to be relatively irradiance-insensitive at $E_0 > 20$ mol quanta $\text{m}^{-2} \text{d}^{-1}$ (see also Morel 1991). Removing the effect of β_d on the irradiance-dependent function of the VGPM increases PP_{annu} by 4.4 Pg C yr^{-1} (total = 47.9 Pg C yr^{-1}) and enhances model sensitivity to clouds (i.e. $PP_{\text{annu}} = 50.4$ Pg C yr^{-1} for clear skies and no β_d). Although these effects of β_d are of secondary importance to P_{opt}^B , they are of concern because β_d is perhaps the most poorly estimated photosynthetic variable measured by long-term ^{14}C incubations. Associated errors may reach 100% in certain cases. Photoinhibition results from exposure to superoptimal PAR or ultraviolet radiation intensities and is dependent on both dose and dose-rate (Prášil et al. 1992; Behrenfeld et al. 1993, 1995; Nagy et al. 1995). Accurate assessment of β_d is therefore critically dependent on matching incubation and in situ light exposures, a criterion that is generally not met using standard ^{14}C methods and results in overestimates of β_d . Because the goal of productivity modeling is to estimate productivity in situ rather than to simply reproduce ^{14}C uptake results, β_d models based on in situ methodologies that do not require incubations should be developed.

Conclusions

The development of ocean productivity models has followed a course of increasing complexity in an attempt to account for unexplained variance between measured and modeled PP_{eu} . However, it is often not clear whether the added complexity reflects more our level of understanding about particular model variables than the importance of their exact representation to predictive capacities of the model. Consequently, there has been a tendency to develop models with increased computational overheads that do not necessarily correspond to increased model performance. We developed a dataset of ^{14}C -based productivity measurements to evaluate which factors, in addition to surface chlorophyll concentrations, were responsible for observed variability in PP_{eu} . We found that scaling a simple formulation for the relative vertical distribution of primary production by the measured optimal assimilation efficiencies (P_{opt}^B) accounted for 86% of the measured variability in PP_{eu} . These results indicate that productivity algorithm performance is primarily dependent on the accuracy to which P_{opt}^B can be modeled. We suggest that improvements in P_{opt}^B estimates require that ecophysiological approaches be adopted that consider how spatial variability in the physical and chemical characteristics of different water bodies acts upon the physiological state of natural phytoplankton assemblages. In other words, improvement of productivity algorithms is dependent not on improved mathematical formulation or finer detail in the

physics of light attenuation and absorption, but on improvement in our understanding of phytoplankton ecology and photophysiology.

We may eventually look back to these early years of satellite oceanography and see that ocean color images, while providing an unparalleled tool for global scale modeling, misled investigation of the factors controlling phytoplankton production in the sea by focusing too much attention toward pigments. Association of pigments with photosynthesis has apparently misguided modeling efforts toward allowing the process of light harvesting to become a primary factor controlling variability in estimated production. From an ecological perspective, light-harvesting capacity rarely, if ever, controls variability in P_{opt} . Compared to terrestrial plants, phytoplankton can experience tremendous variability in light availability and thus they have developed elaborate mechanisms to adjust their light-harvesting capacity to match changes in irradiance at different time scales (Falkowski 1994; Geider et al. 1996). It is therefore reasonable to think that production rates of phytoplankton are governed by basic physical and chemical attributes within their immediate environment and to view the light-harvesting components of photosynthesis as simply dynamic cellular machinery for maintaining a sufficient flow of photochemical energy (over a range of light intensities) to match the requirements for the maximum possible growth rate dictated by these basic environmental constraints. Such a perspective negates the importance of light harvesting on variability in P_{opt} and focuses our attention on identifying the physical and chemical constraints of different systems. We must keep in mind that the photophysiological characteristics of phytoplankton within a given region are expressions of physiological adjustment to a multidimensional suite of environmental factors dictating the growth conditions experienced in situ at a given moment.

References

- ANTOINE, D., J.-M. ANDRÉ, AND A. MOREL. 1996. Oceanic primary production 2. Estimation at global scale from satellite (coastal zone color scanner) chlorophyll. *Global Biogeochem. Cycles* **10**: 57–69.
- BABIN, M., AND OTHERS. 1996. Nitrogen- and irradiance-dependent variations of the maximum quantum yield of carbon fixation in eutrophic, mesotrophic and oligotrophic marine systems. *Deep-Sea Res.* **43**: in press.
- BAKUN, A. 1990. Global climate change and intensification of coastal ocean upwelling. *Science* **247**: 198–201.
- BALCH, W. M., AND C. F. BYRNE. 1994. Factors affecting the estimate of primary production from space. *J. Geophys. Res.* **99**: 7555–7570.
- BALCH, W., AND OTHERS. 1992. The remote sensing of ocean primary productivity: Use of new data compilation to test satellite algorithms. *J. Geophys. Res.* **97**: 2279–2293.
- BANNISTER, T. T. 1974. Production equations in terms of chlorophyll concentration, quantum yield, and upper limit to production. *Limnol. Oceanogr.* **19**: 1–12.
- BANSE, K., AND M. YONG. 1990. Sources of variability in satellite-derived estimates of phytoplankton production in the eastern tropical Pacific. *J. Geophys. Res.* **95**: 7201–7215.
- BEHRENFELD, M. J., J. W. CHAPMAN, J. T. HARDY, AND H. I. LEE. 1993. Is there a common response to ultraviolet-B radiation by marine phytoplankton? *Mar. Ecol. Prog. Ser.* **102**: 59–68.
- , D. R. S. LEAN, AND H. LEE II. 1995. Ultraviolet-B radiation effects on inorganic nitrogen uptake by natural assemblages of oceanic plankton. *J. Phycol.* **31**: 25–36.
- BERNER, T., Z. DUBINSKY, K. WYMAN, AND P. G. FALKOWSKI. 1989. Photoadaptation and the “package” effect in *Dunaliella tertiolecta* (Chlorophyceae). *J. Phycol.* **25**: 70–78.
- BIDIGARE, R. R., B. B. PRÉZELIN, AND R. C. SMITH. 1992. Bio-optical models and the problems of scaling, p. 175–212. *In* P. G. Falkowski [ed.], Primary productivity and biogeochemical cycles in the sea. Plenum.
- BISHOP, J. K. B., AND W. B. ROSSOW. 1991. Spatial and temporal variability of global surface solar irradiance. *J. Geophys. Res.* **96**: 16,839–16,858.
- CAMPBELL, E. J., AND J. E. O'REILLY. 1988. Role of satellites in estimating primary productivity on the northwest Atlantic continental shelf. *Cont. Shelf Res.* **8**: 179–204.
- CHALUP, M. S., AND E. A. LAWS. 1990. A test of the assumptions and predictions of recent growth models with the marine phytoplankton *Pavlova lutheri*. *Limnol. Oceanogr.* **35**: 583–596.
- CLAUSTRE, H., AND J. C. MARTY. 1995. Specific phytoplankton biomasses and their relation to primary production in the tropical North Atlantic. *Deep-Sea Res.* **42**: 1,475–1,493.
- CLARKE, G. L., G. C. EWING, AND C. J. LORENZEN. 1970. Spectra of backscattered light from the sea obtained from aircraft as a measure of chlorophyll concentration. *Science* **167**: 1119–1121.
- CULLEN, J. J. 1990. On models of growth and photosynthesis in phytoplankton. *Deep-Sea Res.* **37**: 667–683.
- , AND M. R. LEWIS. 1988. The kinetics of algal photoadaptation in the context of vertical mixing. *J. Plankton Res.* **10**: 1039–1063.
- DAVISON, I. R. 1991. Environmental effects on algal photosynthesis: Temperature. *J. Phycol.* **27**: 2–8.
- EPPLEY, R. W. 1972. Temperature and phytoplankton growth in the sea. *Fish. Bull.* **70**: 1063–1085.
- , AND B. J. PETERSON. 1979. Particulate organic matter flux and planktonic new production in the deep ocean. *Nature* **282**: 677–680.
- , E. STEWART, M. R. ABBOTT, AND V. HEYMAN. 1985. Estimating ocean primary production from satellite chlorophyll, introduction to regional differences and statistics for the Southern California Bight. *J. Plankton Res.* **7**: 57–70.
- FALKOWSKI, P. G. 1980. Light-shade adaptation in marine phytoplankton, p. 99–119. *In* P. G. Falkowski [ed.], Primary productivity in the sea. Plenum.
- . 1981. Light-shade adaptation and assimilation numbers. *J. Plankton Res.* **3**: 203–216.
- . 1984. Physiological responses of phytoplankton to natural light regimes. *J. Plankton Res.* **6**: 295–307.
- . 1994. The role of phytoplankton photosynthesis in global biogeochemical cycles. *Photosyn. Res.* **39**: 235–258.
- , AND J. LAROCHE. 1991. Acclimation to spectral irradiance in algae. *J. Phycol.* **27**: 8–14.
- , AND T. G. OWENS. 1980. Light-shade adaptation. Two strategies in marine phytoplankton. *Plant Physiol.* **66**: 592–595.
- , ———, A. C. LEY, AND D. C. MAUZERALL. 1981. Effects of growth irradiance levels on the ratio of reaction centers in two species of marine phytoplankton. *Plant Physiol.* **68**: 969–973.
- FITZWATER, S. E., G. A. KNAUER, AND J. H. MARTIN. 1982. Metal contamination and its effects on primary production measurements. *Limnol. Oceanogr.* **27**: 544–551.
- GALLÉGOS, C. L. 1992. Phytoplankton photosynthesis, productivi-

- ty, and species composition in a eutrophic estuary: Comparison of bloom and non-bloom assemblages. *Mar. Ecol. Prog. Ser.* **81**: 257-267.
- GEIDER, R. J., H. L. MACINTYRE, AND T. M. KANA. 1996. A dynamic model of photoadaptation in phytoplankton. *Limnol. Oceanogr.* **41**: 1-15.
- , AND T. PLATT. 1986. A mechanistic model of photoadaptation in microalgae. *Mar. Ecol. Prog. Ser.* **30**: 85-92.
- , ———, AND J. A. RAVEN. 1986. Size dependence of growth and photosynthesis in diatoms: a synthesis. *Mar. Ecol. Prog. Ser.* **30**: 93-104.
- GORDON, H., AND D. K. CLARK. 1980a. Atmospheric effects in the remote sensing of phytoplankton pigments. *Boundary-Layer Meteorol.* **18**: 299-313.
- , AND ———. 1980b. Remote sensing optical properties of a stratified ocean: An improved interpretation. *Appl. Opt.* **19**: 3428-3430.
- , AND ———. 1981. Clear water radiances for atmospheric correction of coastal zone color scanner imagery. *Appl. Opt.* **20**: 4175-4180.
- , AND OTHERS. 1983. Phytoplankton pigment concentrations in the Middle Atlantic Bight: Comparison of ship determinations and CZCS estimates. *Appl. Opt.* **22**: 20-36.
- HENLEY, W. J. 1993. Measurement and interpretation of photosynthetic light-response curves in algae in the context of photoinhibition and diel changes. *J. Phycol.* **29**: 729-739.
- HERZIG, R., AND P. G. FALKOWSKI. 1989. Nitrogen limitation of *Isochrysis galbana* (Haptophyceae). 1. Photosynthetic energy conversion and growth efficiencies. *J. Phycol.* **25**: 462-471.
- HOLM-HANSEN, O., C. J. LORENZEN, R. W. HOLMES, AND J. D. H. STRICKLAND. 1965. Fluorometric determination of chlorophyll. *J. Cons. Int. Explor. Mer* **39**: 3-15.
- JØRGENSEN, E. G. 1968. The adaptation of plankton algae. 2. Aspects of the temperature adaptation of *Skeletonema costatum*. *Physiol. Plant.* **21**: 423-427.
- KAMYKOWSKI, D., AND S.-J. ZENTARA. 1986. Predicting plant nutrient concentrations from temperature and sigma- t in the upper kilometer of the world ocean. *Deep-Sea Res.* **33**: 89-105.
- KIRK, J. T. O. 1994. Light and photosynthesis in aquatic ecosystems, 2nd ed. Cambridge.
- LANDE, R., AND M. R. LEWIS. 1989. Models of photoadaptation and photosynthesis by algal cells in a turbulent mixed layer. *Deep-Sea Res.* **36**: 1161-1175.
- LEWIS, M., R. E. WARNOCK, AND T. PLATT. 1987. Photosynthetic response of marine picoplankton at low photon flux, p. 235-250. *In* Photosynthetic picoplankton. *Can. Bull. Fish. Aquatic Sci.* 214.
- LI, W. K. W. 1980. Temperature adaptation in phytoplankton: cellular and photosynthetic characteristics, p. 259-279. *In* P. G. Falkowski [ed.], Primary productivity in the sea. Plenum.
- LINDSTROM, E., AND OTHERS. 1987. The western equatorial Pacific Ocean circulation study. *Nature* **330**: 533-537.
- LONGHURST, A., S. SATHYENDRANATH, T. PLATT, AND C. CAVERHILL. 1995. An estimate of global primary production in the ocean from satellite radiometer data. *J. Plankton Res.* **17**: 1245-1271.
- LURIN, B., S. I. RASOOL, W. CRAMER, AND B. MOORE. 1994. Global terrestrial net primary production. *Global Change Newlett. (IGBP)* **19**: 6-8.
- MCCBRIDE, G. B. 1992. Simple calculation of daily photosynthesis by means of five photosynthesis-light equations. *Limnol. Oceanogr.* **37**: 1796-1808.
- MANABE, S., AND R. T. WETHERALD. 1974. The effects of doubling the CO₂ concentration on the climate of a general circulation model. *J. Atmos. Sci.* **32**: 3-15.
- MAXWELL, D. P., S. FALK, AND N. P. A. HUNER. 1995. Photosystem-II excitation pressure and development of resistance to photoinhibition 1. Light-harvesting complex-II abundance and zeaxanthin content in *Chlorella vulgaris*. *Plant Physiol.* **107**: 687-694.
- MOREL, A. 1978. Available, usable, and stored radiant energy in relation to marine photosynthesis. *Deep-Sea Res.* **25**: 673-688.
- . 1988. Optical modeling of the upper ocean in relation to its biogenous matter content (case one waters). *J. Geophys. Res.* **93**: 10,749-10,768.
- . 1991. Light and marine photosynthesis: A spectral model with geochemical and climatological implications. *Prog. Oceanogr.* **26**: 263-306.
- , AND J.-F. BERTHON. 1989. Surface pigments, algal biomass profiles, and potential production of the euphotic layer: Relationships reinvestigated in view of remote-sensing applications. *Limnol. Oceanogr.* **34**: 1545-1562.
- , AND L. PRIEUR. 1977. Analysis of variations in ocean color. *Limnol. Oceanogr.* **22**: 709-722.
- , AND R. C. SMITH. 1974. Relation between total quanta and total energy for aquatic photosynthesis. *Limnol. Oceanogr.* **19**: 591-600.
- NAGY, L., AND OTHERS. 1995. Photoinhibition and law of reciprocity in photosynthetic reactions of *Synechocystis sp.* PCC 6803. *J. Plant Physiol.* **145**: 410-415.
- O'REILLY, J. E., AND D. A. BUSCH. 1984. Phytoplankton primary production on the northwestern Atlantic shelf. *Rapp. P.V. Cons. Int. Explor. Mer* **183**: 255-268.
- , C. EVANS-ZETLIN, AND D. A. BUSCH. 1987. Primary production, p. 220-233. *In* R. H. Backus [ed.], Georges Bank. MIT.
- ORELLANA, M., AND M. J. PERRY. 1992. An immunoprobe to measure Rubisco concentration and maximal photosynthetic rates of individual phytoplankton cells. *Limnol. Oceanogr.* **37**: 478-490.
- PLATT, T. 1986. Primary production of the ocean water column as a function of surface light intensity. Algorithms for remote sensing. *Deep-Sea Res.* **33**: 149-163.
- , C. CAVERHILL, AND S. SATHYENDRANATH. 1991. Basin-scale estimates of oceanic primary production by remote sensing: The North Atlantic. *J. Geophys. Res.* **96**: 15,147-15,159.
- , C. L. GALLEGOS, AND W. G. HARRISON. 1980. Photoinhibition of photosynthesis in natural assemblage of marine phytoplankton. *J. Mar. Res.* **38**: 687-701.
- , AND S. SATHYENDRANATH. 1988. Oceanic primary production: Estimation by remote sensing at local and regional scales. *Science* **241**: 1613-1620.
- , AND OTHERS. 1992. Nutrient control of phytoplankton photosynthesis in the western North Atlantic. *Nature* **356**: 229-231.
- , AND D. V. SUBBA RAO. 1975. Primary production of marine microphytes, p. 249-280. *In* J. P. Cooper [ed.], Photosynthesis and productivity in different environments. Cambridge.
- PRASIL, O., N. ADIR, AND I. OHAD. 1992. Dynamics of photosystem II: Mechanism of photoinhibition and recovery processes, p. 295-348. *In* J. Barber [ed.], The photosystems: Structure, function and molecular biology. Elsevier.
- RODHE, W., R. A. VOLLENWEIDER, AND A. NAUWERK. 1958. The primary production and standing crop of phytoplankton, p. 299-322. *In* A. A. Buzzati-Traverso [ed.] Perspectives in marine biology. Univ. Calif.
- RYTHER, J. H., AND C. S. YENTSCH. 1957. The estimation of phytoplankton production in the ocean from chlorophyll and light data. *Limnol. Oceanogr.* **2**: 281-286.
- SAKSHAUG, E., AND K. ANDRESEN. 1986. Effect of light regime upon growth rate and chemical composition of a clone of *Ske-*

- letonema costatum* from the Trondheimsfjord, Norway. J. Plankton Res. **8**: 619–637.
- , D. A. KIEFFER, AND K. ANDRESEN. 1989. A steady state description of growth and light absorption in the marine planktonic diatom *Skeletonema costatum*. Limnol. Oceanogr. **34**: 198–205.
- SARMIENTO, J. L., J. C. ORR, AND U. SIEGENTHALER. 1992. A perturbation simulation of CO₂ uptake in an ocean general circulation model. J. Geophys. Res. **94**: 3621–3645.
- , AND U. SIEGENTHALER. 1992. New production and the global carbon cycle, p. 317–332. In P. G. Falkowski and A. D. Woodhead [eds.], Primary productivity and biogeochemical cycles in the sea. Plenum.
- SATHYENDRANATH, S., AND T. PLATT. 1993. Remote sensing of water-column primary production. ICES Mar. Sci. Symp. **197**: 236–243.
- SMITH, R. C., AND K. S. BAKER. 1978. The bio-optical state of ocean waters and remote sensing. Limnol. Oceanogr. **23**: 247–259.
- , R. W. EPPLEY, AND K. S. BAKER. 1982. Correlation of primary production as measured aboard ship in southern California coastal waters and as estimated from satellite chlorophyll images. Mar. Biol. **66**: 281–288.
- STEEHMANN NIELSEN, E. 1952. The use of radio-active carbon (C¹⁴) for measuring organic production in the sea. J. Cons. Cons. Int. Explor. Mer **18**: 117–140.
- SUKENIK, A., J. BENNETT, AND P. G. FALKOWSKI. 1987. Light-saturated photosynthesis-limitation by electron transport or carbon fixation? Biochim. Biophys. Acta **891**: 205–215.
- TALLING, J. F. 1957. The phytoplankton population as a compound photosynthetic system. New Phytol. **56**: 133–149.
- THURMAN, H. V. 1985. Introductory oceanography, 4 ed. Merrill.
- WALSH, J. J. 1984. The role of ocean biota in accelerated ecological cycles: A temporal view. BioScience **43**: 499–507.
- WIRICK, C. D. 1994. Exchange of phytoplankton across the continental shelf-slope boundary of the Middle Atlantic Bight during spring 1988. Deep-Sea Res. **41**: 391–410.
- WRIGHT, J. C. 1959. Limnology of Canyon Ferry Reservoir: Phytoplankton standing crop and primary production. Limnol. Oceanogr. **4**: 235–245.
- ZENTARA, S.-J., AND D. KAMYKOWSKI. 1977. Latitudinal relationships among temperature and selected plant nutrients along the west coast of North and South America. J. Mar. Res. **35**: 321–337.

Submitted: 8 December 1995

Accepted: 2 May 1996

Amended: 9 October 1996